UNCLASSIFIED
SECURITY CLASSIFICATION OF THIS PAGE

MENTATION PAGE

Form Approved
OMB No 0704-0188

AD-A208 655

1a. R

1b RESTRICTIVE MARKINGS

2a. SI

3 DISTRIBUTION/AVAILABILITY OF REPORT

2b. DECLASSIFICATION/DOWNGRADING SCHEDULE

4. PERFORMING ORGANIZATION REPORT NUMBER(S)

5 MONITORING ORGANIZATION REPORT NUMBER(S)
AFOSR-TR- 89-0720

6a. NAME OF PERFORMING ORGANIZATION	6b. OFFICE SYMBOL (If applicable)	7a. NAME OF MONITORING ORGANIZATION
R&D Associates Washington Research Laboratory		Air Force Office of Scientific Research Building 410
6c. ADDRESS (City, State, and ZIP Code)		**7b. ADDRESS (City, State, and ZIP Code)**
301 S. West Street Alexandria, VA 22314		Bolling Air Force Base, DC 20332-6448

8a. NAME OF FUNDING/SPONSORING ORGANIZATION	8b. OFFICE SYMBOL (If applicable)	9. PROCUREMENT INSTRUMENT IDENTIFICATION NUMBER
Same as 7a	NP	F49620-87-C-0006
8c. ADDRESS (City, State, and ZIP Code)		**10. SOURCE OF FUNDING NUMBERS**
Same as 7b		PROGRAM ELEMENT NO. 63220C; PROJECT NO. D812 D812; TASK NO. F1 B1; WORK UNIT ACCESSION NO.

11. TITLE (Include Security Classification)
(U) Dense Plasma Jet Propagation for Endoatmospheric Ballistic Missile Defense.

12. PERSONAL AUTHOR(S)
RDA Washington Research Laboratory Staff

13a. TYPE OF REPORT	13b. TIME COVERED	14. DATE OF REPORT (Year, Month, Day)	15. PAGE COUNT
FINAL	FROM 1 Oct 86 TO 30 Jun88	June 1988	80

16. SUPPLEMENTARY NOTATION

17. COSATI CODES			18. SUBJECT TERMS (Continue on reverse if necessary and identify by block number)
FIELD	GROUP	SUB-GROUP	Jets and Plasmas

19. ABSTRACT (Continue on reverse if necessary and identify by block number)

The present research effort has been developing the experimental conditions necessary to achieve reasonable comparison with theoretical predictions for plasma jet propagation in the atmosphere. Time-resolved measurements have been made of high speed argon plasma jets penetrating a helium background (simulating xenon jets propagating into air). Basic radial confinement of the jet has been observed by photography and spectroscopy and structures in the flow field resemble those predicted by numerical calculations. Results from our successful initial experiments have been used to design improved diagnostic procedures and arcjet source characteristics for further experiments.

20 DISTRIBUTION/AVAILABILITY OF ABSTRACT	21. ABSTRACT SECURITY CLASSIFICATION
☒ UNCLASSIFIED/UNLIMITED ☒ SAME AS RPT ☐ DTIC USERS	UNCLASSIFIED

22a. NAME OF RESPONSIBLE INDIVIDUAL	22b. TELEPHONE (Include Area Code)	22c. OFFICE SYMBOL
Lt Col Bruce L. Smith	(202) 767-4908	NP

DD Form 1473, JUN 86 Previous editions are obsolete. SECURITY CLASSIFICATION OF THIS PAGE
UNCLASSIFIED

89 6 06 084

RDA-TR-143700-002

R & D ASSOCIATES

F49620-87-C-0006

FINAL TECHNICAL REPORT

1 Oct 86 - 30 Jun 88

DENSE PLASMA JET PROPAGATION FOR ENDOATMOSPHERIC BALLISTIC MISSILE DEFENSE

Submitted to:

AIR FORCE OFFICE OF SCIENTIFIC RESEARCH
Bolling Air Force Base
Washington, DC 20332-6448

Sponsored by: SDIO/IST

Managed by: AFOSR

Prepared by:

RDA/WRL Staff

TABLE OF CONTENTS

LIST OF ILLUSTRATIONS

I. SUMMARY

A variety of schemes have been proposed over the last two decades for delivering lethal amounts of energy and/or momentum to targets such as missiles and high speed aircraft. Techniques have ranged from high energy lasers and high voltage charged-particle accelerators to less exotic but still challenging devices such as electromagnetic railguns. One class of technology involves the use of high speed plasmas. The primary attraction of such technology is the possibility of utilizing relatively compact accelerators and electrical power systems that could allow highly mobile and agile operation from rocket or aircraft platforms, or in special ordnance.

Two years ago, R & D Associates examined the possibility of plasma propagation for military applications and concluded that the only viable approach consisted of long dense plasma jets, contained in radial equilibrium by the atmosphere, while propagating at speeds of about 10 km/s. Without atmospheric confinement the plasma density would diminish too rapidly for adequate range and lethality. Propagation of atmospherically-confined jets at speeds much greater than 10 km/s required significant increases in power levels and/or operating altitudes to achieve useful ranges. To examine the ability of a hypervelocity plasma jet to propagate in a background atmosphere, RDA proposed a basic research project to AFOSR in 1984. Since that time further impetus for such research has resulted in sponsorship by SDIO/IST.

The present research effort has been developing the experimental conditions necessary to achieve reasonable comparison with theoretical predictions for plasma jet propagation in the atmosphere. Time-resolved measurements have been made of high speed argon plasma jets penetrating a helium background (simulating xenon jets propagating into air). Basic radial confinement of the jet has been observed by photography and spectroscopy and structures in the flow field resemble those predicted by numerical calculations. Results from our successful initial

experiments have been used to design improved diagnostic procedures and arcjet source characteristics for further experiments.

In experiments with a modified arcjet source, radial confinement of the jet is again observed, with the 3 cm exit diameter of the jet preserved downstream for the duration of the quasi-steady flow. The modification of the arcjet consisted of the addition of a converging-diverging nozzle upstream of the 3 cm diam exit of the arcjet to expand the jet further before its entry into the background atmosphere. The jet penetrates for tens of diameters into the target atmosphere at a speed of 2 km/s, with an estimated jet flow speed of 5.3 km/s. The jet diameter is maintained for the range of the jet, which appears to equal 1 to 1.5 times the product of jet penetration speed and pulse duration (~ 350 μs in the present experiments), as expected from theoretical considerations. Further modification of the arcjet source (increasing throat diameter and electrode radius ratio) and extension of the current pulse time are expected to increase the jet range.

II. INTRODUCTION

Defense against missiles travelling at speeds in excess of Mach six will require techniques to deliver lethal amounts of energy at much higher speeds. Various laser and particle beam weapons have been proposed that can provide energy transfer to the target missile at essentially the speed of light. The overall system requirements with such weapons, however, including large mirrors and accelerators, involve concerns of vulnerability and cost-effectiveness that are still being addressed. Similarly, the costs of deployment and utilization of antimissile missile systems are being evaluated along with estimates of potential threats and countermeasures. The use of projectiles launched from guns, such as electromagnetic railguns, has also been proposed and is under evaluation.

A principal difficulty with gun systems is the need for rather long gun barrels (> 10 - 30 m) to achieve projectile speeds comparable to high performance rockets. If lower mass density "projectiles" such as high energy plasmas could be delivered to a target missile, then smaller gun systems (< 1 m) might be possible at very high intercept speeds. The problem with such an approach is that the integrity of the plasma projectile will be lost soon after its release from the accelerating structure. Basically, without the constraint of magnetic fields or mechanical structures, the plasma will expand due to its internal thermal and magnetic energy densities at speeds in excess of about 10 km/s. The resulting loss of energy density then precludes lethal interaction at the target missile. Such expansion is not prevented by the use of so-called "force-free" plasma/field configurations, which still need to be confined by a boundary condition involving external magnetic or mechanical pressure.

A "force-free" plasmoid can be supported (temporarily) by the pressure of a surrounding atmosphere, but high speed motion through such an atmosphere rapidly diminishes the plasmoid's momentum (in a few diameters of travel). To extend the range of

a plasma projectile in a confining atmosphere, it is necessary to increase the effective mass length of the projectile. Launching a "spear" of plasma through a background gas is a process that may be expected to suffer from a number of loss phenomena including viscous diffusion, instabilities and simple changes in projectile shape due to gasdynamic forces. It is possible, however, that the nonlinear development of the flow dynamics, combined with proper scaling of projectile size (e.g., diameter) and density to diminish the effects of diffusive processes may offer a satisfactory solution. The resulting weapon concept would then consist of a plasma source/accelerator injecting hypervelocity plasma into a long jet confined by the surrounding atmosphere. The accelerator would be quite small compared to devices such as railguns, which utilize solid density projectiles, so it could be deployed on mobile platforms (rockets, aircraft) and maneuvered readily. Energy is added to the plasma jet by the accelerator during the course of jet penetration through the atmosphere and could be supplied by relatively modest, pulsed electrical power sources, such as MHD generators. Propagation of a plasma projectile through the atmosphere at Mach thirty should allow reasonable intercept of solid density targets whose speeds are limited to much lower Mach numbers.

Before such system advantages can reasonably be considered, however, it is necessary to examine the basic questions of jet propagation in a background atmosphere. Can a jet that is confined radially by a surrounding gas actually penetrate that same gas for many jet diameters? What are the conditions for jet density and speed that allow efficient propagation of energy over long distances? While the nonlinear dynamics of the jet-atmosphere interactions are quite complex, the experimental requirements to answer the preceding questions can be satisfied rather easily and a body of calculations already exists that offers promise for some success.

III. EXPERIMENTAL APPROACH

The possibility of propagating a hypervelocity plasmajet through the atmosphere has its most dramatic visualization in the color-graphic results (Figure 1) of numerical calculations by Norman, Smarr, and Winkler, who were studying jet propagation in an astrophysical context. In a series of computations on a Cray-1, the behavior of axisymmetric (and also planar) jets were studied for a range of inlet Mach numbers (directed speed divided by sound speed in the jet) and ratios of inlet jet density to ambient density. The calculations were based on inviscid hydrodynamics with an adiabatic, perfect gas law, equation of state. (Even with such idealized fluid mechanics, a typical run required ten to thirty hours). For a range of Mach numbers and density ratios (bounded by regimes of normal shock formation and cocoon development), it appears that the prospect for endoatmospheric jet propagation improves significantly.

To explore such propagation experimentally, it is useful to start in a parameter regime consistent with the computational survey and to adjust experimental conditions to approach the idealizations of computer modeling. Since the Mach numbers and density ratios were varied from $M = 1.5$ to 12, and $\eta = 0.01$ to 10, respectively, experimental values of $M \approx 5$ and $\eta \approx 0.3$ would be appropriate initial goals. These values should provide a jet that is safely below the stability limit-line given by $\eta < (M-1)^2$ and above the less well-defined region of cocoon formation (Figure 2, from Smarr, *et al*). To utilize the two parameters, M and η, as guides for stability, the flow must approach the ideal conditions of the theory.

Reasonable approximation for inviscid flow requires a viscous Reynolds number, Rey, much greater than unity. Collisionality on the scale size of interest is also important and requires low Knudsen number, Kn. The Knudsen and Reynolds number are related through the Mach number: $Kn \approx M/Rey$. For Mach numbers of 5-10, Reynolds numbers in excess of 10^4 are needed

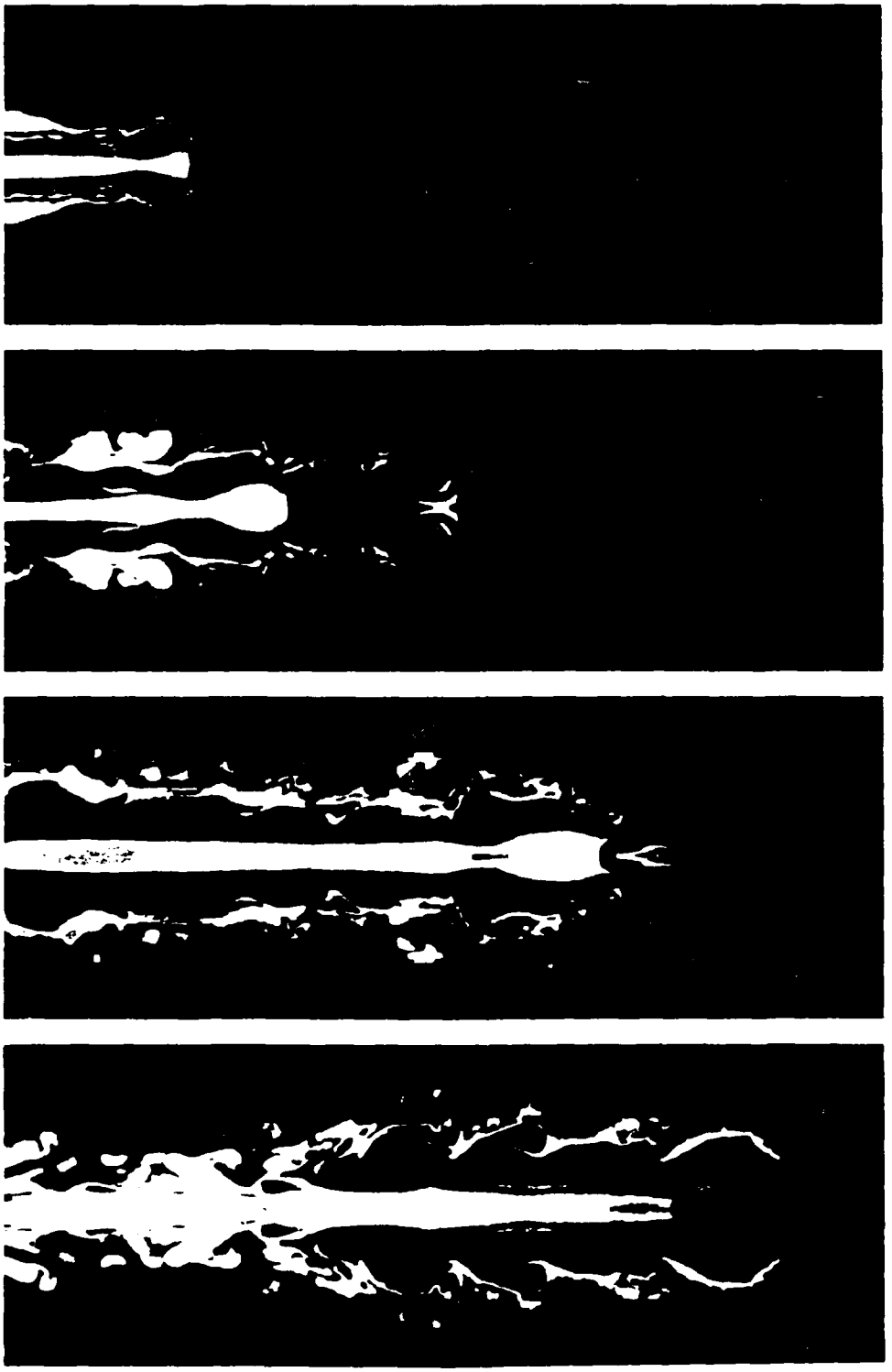

Figure 1. Example of results of numerical calculations by Norman, Smarr, and Winkler. Time evolution of an axisymmetrical jet with M = 6 and η = 0.01. Colors correspond to entropy contours with low to high logarithmic values varying spectrally from blue to red. (From Smarr, Norman, and Winkler, Physica 12D (1984) 83-106. Fig 4.)

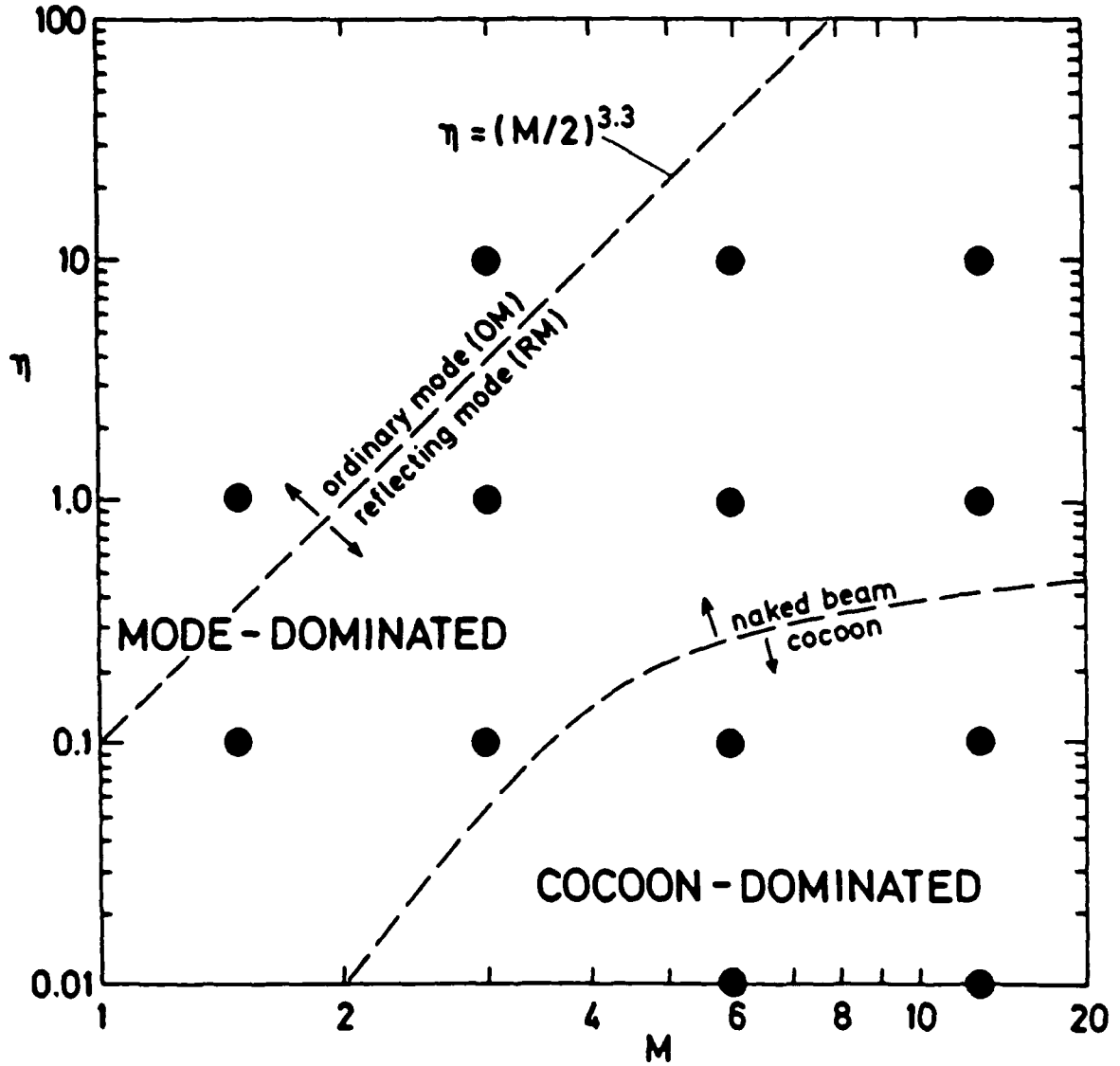

Figure 2. Density ratio η vs Mach number M indicating regions of jet behavior. Stability requires operation below and to right of ordinary mode-dominated regime. (From Smarr, Norman, and Winkler, Physica 12 D (1984) 86-106. Fig 5.)

to keep the Knudsen number safely in the continuum regime $Kn < 10^{-3}$).

While selection of experimental values to achieve high Reynolds number flow will keep the experiment in reasonable agreement with inviscid hydrodynamic theory, the numerical modeling itself deviates from such theory because of finite grid-size and the inclusion of numerical viscosity. Thus a loss of fine scale detail to diffusive processes in the experiment may be (more than) matched by a similar loss to numerical code limitations. The greatest deviation of code from experiment, in any event, will be due to the simplified equation of state and energy transport processes in the code. At the anticipated speeds (> 10 km/s), ionization, excitation, and radiation are important phenomena. The temperature distributions predicted by the code can be considerably inaccurate, but more importantly, structures that depend on pressure conditions (associated with sharp temperature variations) may be absent in the experiment.

Although the equations of state of materials at high temperature can be computed and combined with models for heat transport, it is unlikely that computational time requirements would allow jet propagation calculations to be performed within foreseeable resources (several days of Cray-1 time would probably be needed for each run). Only numerical computation, however, can properly account for the nonlinear structural dynamics of the flow. We must therefore admit that the limit of present calculational ability has been reached in regard to close comparison of theory and experiment. The existing computations provide a base from which experimental exploration can start, but they can only suggest the processes that will determine jet propagation.

IV. EXPERIMENT DESIGN

To estimate the parameters of initial experiments on plasmajet propagation, it is reasonable to start with the desired Mach number and density ratio values and to derive the necessary scale size, power, and energy content required to achieve these values in the context of inviscid, continuum flow. Favorable comparison with the capabilities of existing laboratory apparatus then provides the basis for an experimental program.

Over the last two decades, magnetoplasmadynamic (MPD) arcjets have been studied as candidates for electric rocket thrusters. Typical quasi-steady (millisecond duration) operation has involved currents of 20-60 kA at power levels of 2-20 MW. With heavy propellant gases, such as argon, exhaust speeds have been about 10-30 km/s. Plasma (heavy particle) temperatures are not well-known, but electron temperatures of 1-2 eV have been measured. (For high atomic number plasmas, the heavy particle temperature may range from 0.5 to 10 eV). The estimated Mach number of the exhaust jet is therefore $M \geq 3.6$. It is thus reasonable to expect that Mach numbers in the stable regime ($M \approx 5$ for $\eta \approx .3$) can be obtained using MPD arcjet technology.

The density ratio can be estimated directly from the assumed jet temperature and the selected species for the plasmajet and target atmosphere. For simple pressure equilibrium at the jet exhaust, in line with the numerical modeling, the density ratio merely follows the atomic mass and (inverse-) temperature ratios:

$$\eta = \frac{\rho_J}{\rho_a} = \frac{m_J}{m_a} \frac{T_a}{T_J} \frac{1}{(1 + Z\ T_e/T_J)}$$

where m and T are the atomic masses and temperatures, respectively, and the subscripts, J, a, and e refer to the jet, the ambient-target, and the plasmajet electrons; the number of free electrons per heavy particle that contribute to the jet pressure is given by Z. For argon and/or xenon jets injected into helium, values of density ratio will be $\eta = 0.02$ to 1.7,

for exhaust temperatures ranging from 0.5 to 10 eV. The lowest values of density ratio correspond to the lowest values of Mach number so that the estimated regime of operation would be well away from the normal-shock instability limit-line and in the "naked beam" or cocoon regions depending on the specific mix of values (and the exactness of the boundary between these regions).

To achieve flow conditions that are adequately within the inviscid and continuum regimes at high Mach number requires a viscous Reynolds number, Rey > 10^4. A Reynolds number based on the jet diameter, D, is useful for initial estimates:

$$\text{Rey} = \frac{\rho_J u_J D}{\mu_V}$$

where μ_V is the viscosity and u_J is the exhaust speed. The viscosity of argon displays a factor of ten decrease as the temperature is increased from one to two eV. (This decrease is due to reduced mean free paths associated with the greater importance of Coulomb collisions above 1 eV). If the maximum value for μ_V (in the 0.5-2 eV range) is selected, $\mu_V = 2.6 \times 10^{-4}$ kg/m-s, and an exhaust velocity of 30 km/s is assumed, then the density required to achieve Rey = 10^4 is:

$$\rho_J = \frac{8.7 \times 10^{-5}}{D} \quad [\text{kg/m}^3]$$

$$= 2.9 \times 10^{-3} \text{ kg/m}^3 \ ,$$

for D = 3 cm, which is a convenient experimental value. At a temperature of 1 eV, and assuming an argon plasmajet, the background helium density is about 1.1×10^{-2} kg/m^3, which corresponds to an ambient pressure of 7×10^{-2} atm (= 53 torr). The values of Mach number and density ratio for these conditions are M = 16.5 and $\eta = 0.26$, respectively, and might be altered by the addition of xenon to survey values of η up to 1.7, (depending on experimental variations in other conditions such as jet temperature).

To obtain the momentum flux associated with the assumed velocity and cross-section, and the computed mass density, the

thrust of the arcjet must be:

$$F = \rho_J \, u_J^2 \, \pi D^2/4$$

$$= 1.8 \times 10^3 \text{ nt}$$

The electromagnetic component of thrust from an MPD arcjet is given by:

$$F_{EM} = \frac{\mu_o}{4\pi} J^2 \, (\ell n r_2/r_1 + 3/4)$$

where J is the arcjet current, r_2/r_1 is the ratio of outer-to-inner current attachment radii, and μ_o is the permeability of free space. For the quantity in parenthesis equal to two, the necessary arcjet current is J = 96 kA.

The kinetic power in the exhaust is:

$$P_K = \frac{1}{2} F \, u_J$$

$$= 27 \text{ Mw.}$$

Typically, the efficiency for conversion of electromagnetic power to thrust power in MPD arcjets is greater than 25%, so the electrical input power required would be less than about 108 Mw(e). At a current of 96 kA, the effective impedance of the arcjet is 12 mΩ and the voltage drop is less than 1200 V.

The head of the jet will penetrate into the ambient gas at a speed that is less than the exhaust speed. In the limit of high Mach number, the contact surface between the (shock-accelerated) ambient gas and the (shock-decelerated) jet material will move at a speed u_{CS} given by:

$$\rho_J (u_J - u_{CS})^2 = \rho_a \, u_{CS}^2$$

so

$$\frac{u_{CS}}{u_J} = \frac{\eta^{\frac{1}{2}}}{1+\eta^{\frac{1}{2}}} \quad .$$

With $\eta = 0.26$, $u_{CS} = 0.34 \, u_J$, so the assumed exhaust speed of 30 km/s will provide a penetration speed of about 10 km/s. The time to propagate a hundred initial diameters is therefore about

300 μs, so the total electrical energy delivered to the arcjet is about 32 kJ.

The conditions for initial experimental tests of endoatmospheric plasmajet propagation are summarized in Table I.

TABLE I

Argon Jet into Helium Atmosphere

Jet Conditions		Electrical Requirements	
Mach Number	= 16.5	Arcjet Current	= 96 kA
Density Ratio	= 0.26	Arcjet Voltage	= 1200 V
Reynolds Number	= 10^4	Effective Impedance	= 12 mΩ
Knudsen Number	= 1.65×10^{-3}	Input Power	$\leq$ 108 Mw
Exhaust Speed	= 30 km/s	Pulse Duration	$\geq$ 300 μs
Contact Speed	= 10 km/s	Input Energy	= 32 kJ
Initial Diameter	= 3 cm	(for 100-diam long jet)	

These values are consistent with existing equipment at the RDA Washington Research Laboratory. The experiments can be performed within the 0.6 x 6 m vacuum facility presently used for AFOSR-sponsored arcjet studies. This facility is adjacent to a 400 kJ, 20 kV capacitor bank capable of providing currents up to 1 MA in a LRC-circuit. The bank is presently configured as an LC-ladder pulse forming network and provides a reasonably constant current pulse with peak amplitude of 53 kA and pulsewidth of about 400 μs. Higher currents for similar pulsetimes may be possible by reconfiguring the bank with a crow-bar switch to allow currents of a few hundred kiloamperes (but with an exponentially decaying waveform). An additional 6 meter long section of vacuum tank is available at RDA/WRL to extend the propagation length to 12 meters (400 initial diameters).

By assembling a 5 MJ, 12 kV capacitor bank from components existing at RDA/WRL, it would be possible to increase the total jet energy by an order of magnitude. Such an increase would permit studies at higher mass densities and/or larger initial diameters to approach more closely the inviscid, continuum flow regime (e.g., by increasing Reynolds number by an order of magnitude). Furthermore, for the jet conditions given in Table I, the larger bank would allow the jet length to be increased to the available vacuum tank dimensions with less impact on the stored energy driving the arcjet.

Use of heavier jet materials, such as xenon, may provide higher Mach numbers and density ratios. Operation at the same particle densities and exhaust speeds with xenon vs argon would immediately require a factor of more than three in energy supplied by the power source. Propagation of heavier jets at the same speed into heavier target atmospheres such as air would also require the extension of the power supply to higher energies. In Table II, as an example, conditions are summarized for testing a xenon plasmajet (at T_J = 0.5 eV) into a target of air.

TABLE II

Xenon Jet into Air

(at 20 km Equivalent Altitude)

Jet Conditions		Electrical Requirements	
Mach Number	= 43.5	Arcjet Current	= 268 kA
Density Ratio	= 0.23	Arcjet Voltage	= 3.3 kV
Reynolds Number	= 4.4×10^4	Effective Impedance	= 12 mΩ
Knudsen Number	= 10^{-3}	Input Power	≤ 866 Mw
Exhaust Speed	= 30 km/s	Pulse Duration	= 1.2 ms
Contact Speed	= 10 km/s	Input Energy	= 1 MJ
Initial Diameter	= 3 cm	(for 400-diam long jet)	

It is interesting to note that the dynamic pressure $\rho_J u_J^2$ for the jet in Table II is 204 atm (3000 psi). The kinetic energy flux $\rho_J u_J^3/2$ is 300 Gw/m^2, which is equivalent to a blackbody temperature of 4 eV. At these levels of pressure and energy flux, significant solid target degradation should be expected. Depending on the details of the jet-surface interaction, surface evaporation under such extreme power flux loadings could result in local failure due to pressures in excess of 2000 atm. Experimental operation with the 5 MJ power source and the values of Table II would allow examination of plasmajet lethality under conditions approaching actual use for high altitude endoatmospheric intercept.

For the experiments described in Sections V and VI, the current and voltage characteristics of the arcjet source are essentially unchanged (as the nozzle region of the arcjet is modified). In Figures 3-5, the current, terminal voltage and power to the arcjet are displayed. (The power is merely the product of voltage and current.) The terminal voltage includes the anode and cathode fall voltages in addition to the resistive and back EMF contributions across the plasma flow. The electromagnetic thrust equation is related only to the back EMF, due to plasma flow in a magnetic field (i.e., $\bar{u}x\bar{B}$). The resistive component of the voltage and a portion of the electrode fall voltages contribute to the thermal energy of the flow, which can be partially converted to directed kinetic energy by flow expansion.

The design of the initial arcjet source is based on experience with similar systems over the last twenty years. In particular, it was recognized that rather simple arrangements would provide adequate performance without delaying experimental progress to deal with long term concerns such as insulator or electrode erosion. Accordingly, the electrodes were made of brass and the insulator (backplate) through which mass is injected was made of Plexiglas. Figure 6 provides a schematic view of the initial arcjet source, which is shown in exploded view in Figure 7. The electrodes assemble into a nested conical

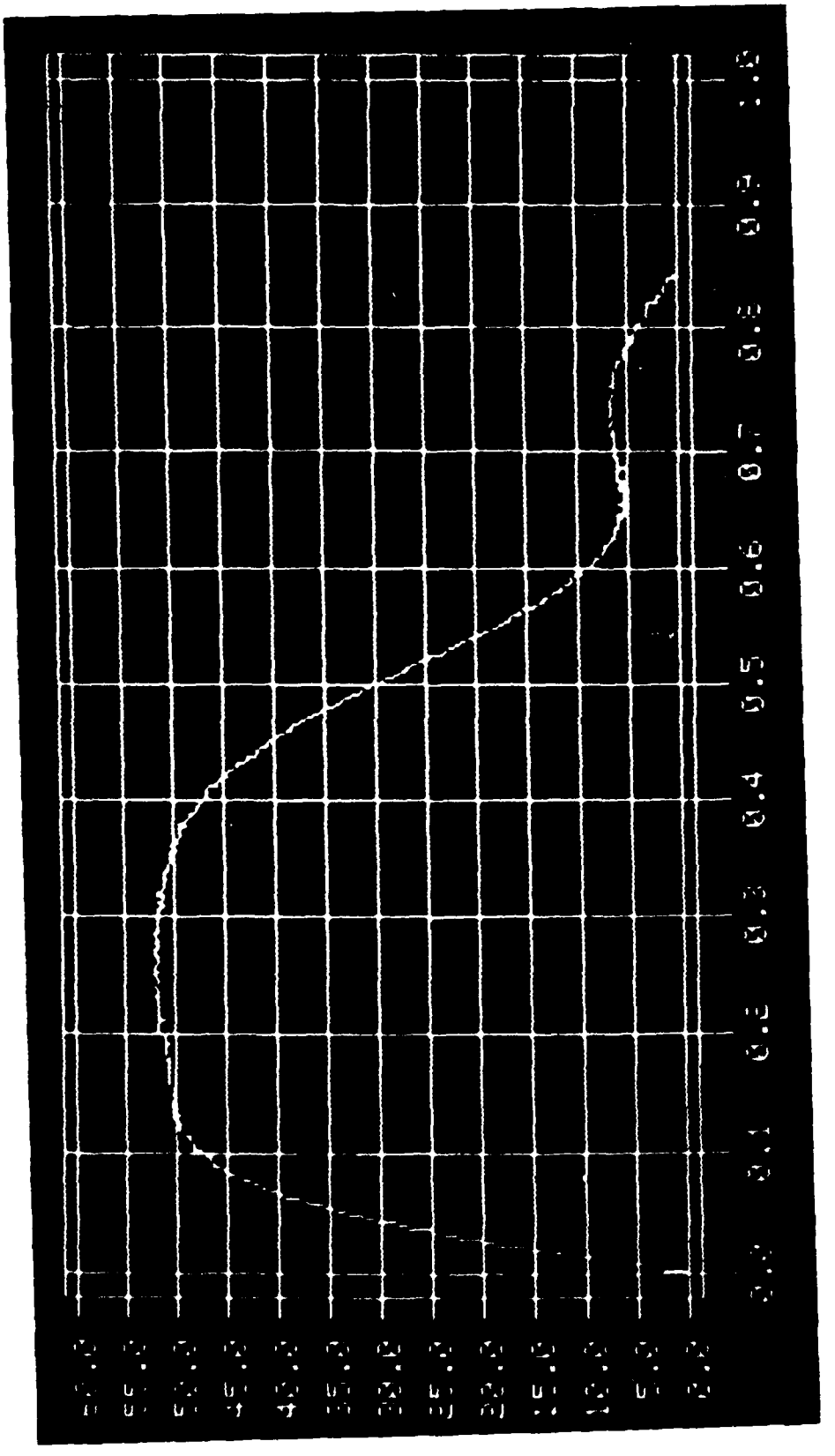

Figure 3. Current delivered to the dense plasmajet rises to 50-53 kA in 100 µs and is approximately level for 300 µs.

Figure 4. Voltage measured at the breech of the dense plasmajet shows an initial transient that becomes quasi-steady at 105-110 volts after 100 μs of current start and remains steady for the pulse duration.

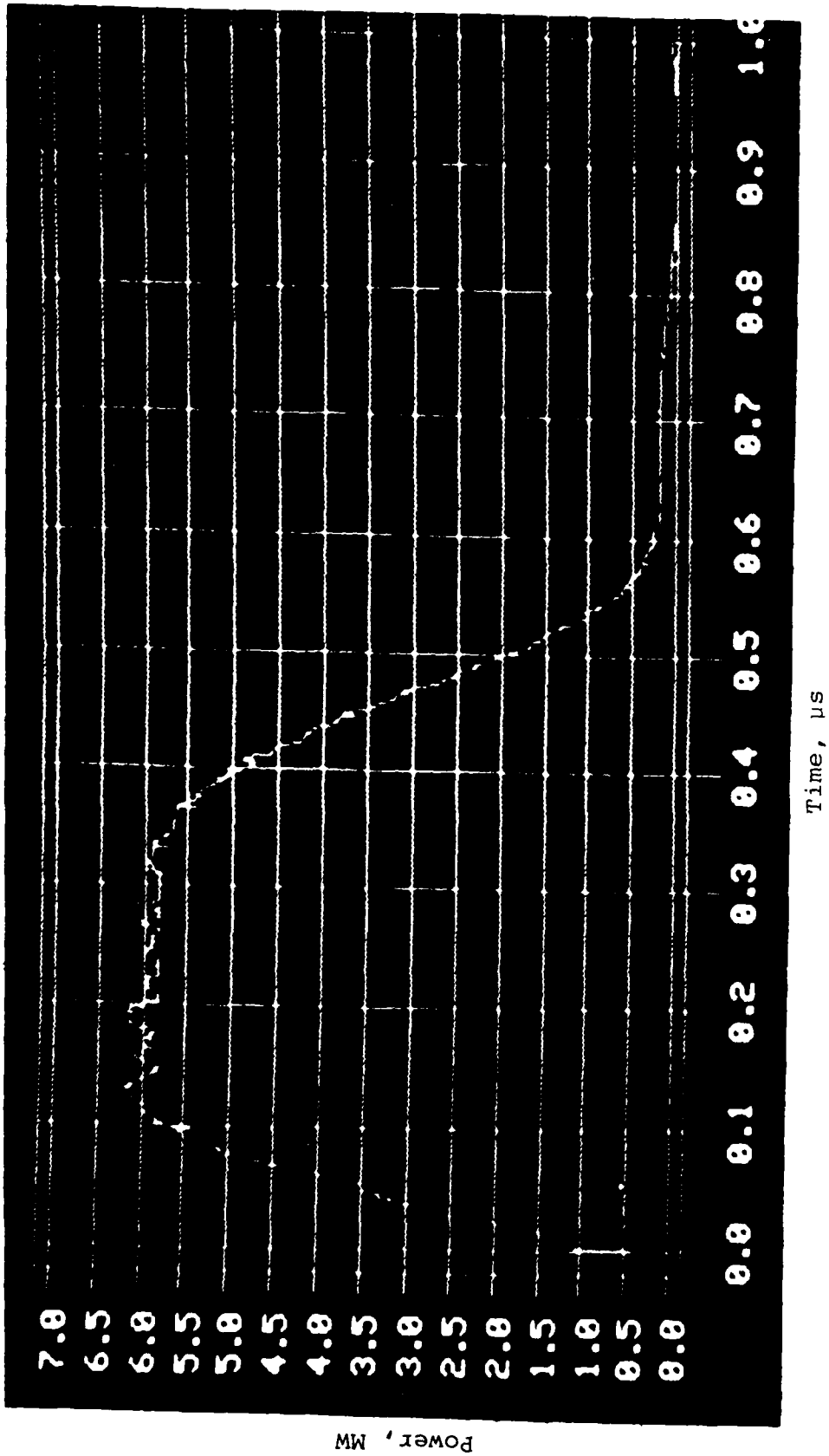

Figure 5. For laboratory experiments, quasi-steady plasmajet operation permits investigation of high power density jet propagation (Gw/m^2) at modest total energies (2 kJ).

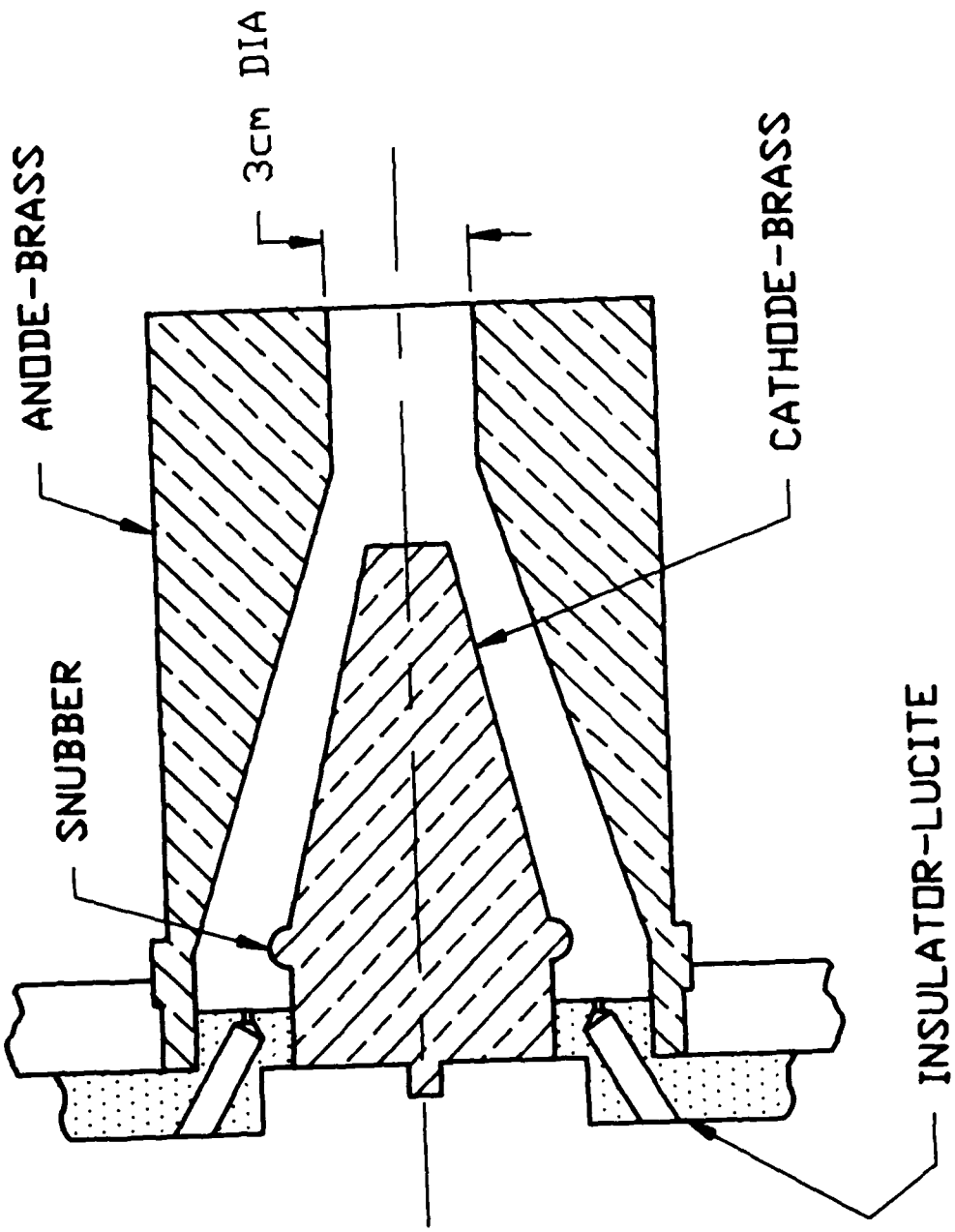

Figure 6. Schematic diagram of initial arcjet source used in dense plasma jet studies.

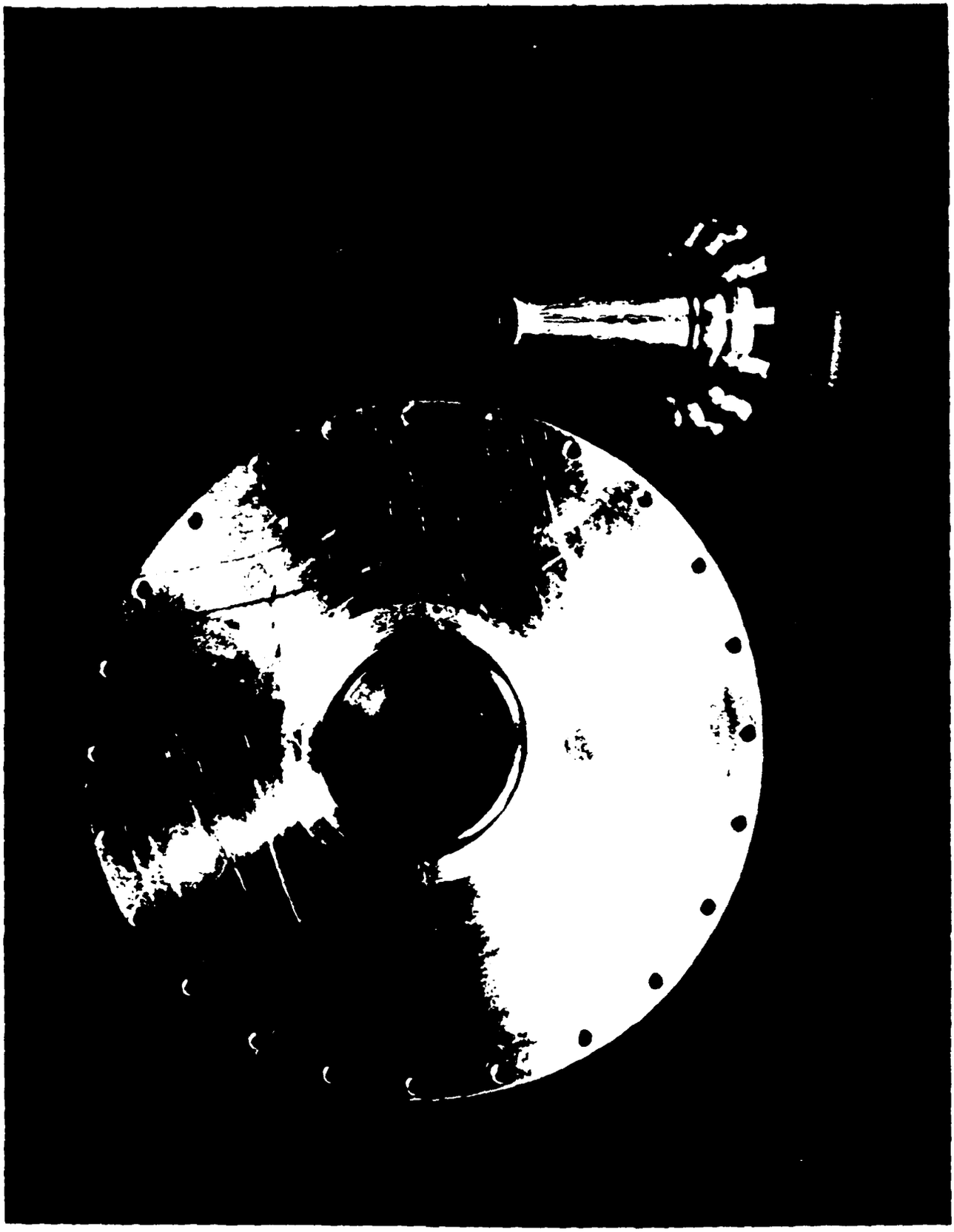

Figure 7. Dense plasmajet electrodes and Plexiglas back plate with the gas injection ports used in initial propagation experiments.

arrangement that allows the diffuse arc processes (largely in the snubber region off the backplate) to provide a high speed flow into the smaller area exhaust region. Concentration of the flow is required to achieve the necessary thrust density estimated for penetration of the target atmosphere in a reasonably continuum flow process. In principal, it is possible to perform a detailed analysis of the arcjet internal flow in order to improve efficiency, flow speed and lifetime. Such an analysis would require a two-dimensional MHD code with real gas chemistry and electrode physics, and is beyond the resources of the present effort. Rapid modification of the simple design based on experimental performance should be sufficient, however, to permit early progress.

The basic operation of the experiment consists of the following procedures. After assembly of the arcjet source in the 0.6 x 6 meter tank, vacuum conditions (~ 10^{-6} torr) are established in order to remove spurious gases. The tank is then backfilled with the desired pressure of target atmosphere. A reservoir for the arcjet mass flow is also filled. The reservoir is separated from the injection ports (in the insulator backplate) by six fast solenoid-actuated valves and a settling plenum. The pressure in the reservoir is set to provide the desired mass flow rate based on previous measurements of pressure vs time in the plenum, and the condition of choked-flow through the injection holes into the arcjet chamber. The capacitor bank PFN is charged to the necessary initial voltage and discharged through a matching resistor and the arcjet after delaying a specified time from the firing pulse to the gas valves (usually from the rotating mirror camera system). The optical rotating-mirror framing camera is used to obtain time-resolved, spatially-resolved images of the plasma jet penetrating the target atmosphere. A variety of other diagnostics, including current and voltage monitors, microchannel plate image converter cameras and spectrographs are also utilized.

The basic experimental program in the near term consists of adjusting the mass flow rate and target atmosphere pressure in

order to achieve a propagating high speed jet. Modifications of the arcjet source are also made to adjust the jet temperature and directed speed. More detailed examinations of the flow structure, properties (densities and temperatures) and scaling relationships (e.g., range vs target pressure) are then conducted in the vicinity of the regime of successful jet propagation.

V. INITIAL EXPERIMENTS

The first experiments to examine dense plasma jet propagation in a background atmosphere utilized the constant exit bore arcjet design shown in Figure 6. Initial tests were performed with the LC-ladder configuration of the capacitor bank arranged to provide twice the pulse width and half the current level of the waveform in Figure 3 (which was used in later tests). Operation of the arcjet source with argon propellant into vacuum (i.e., no background atmosphere) displayed optical exhaust patterns typical of unimpeded plasma expansion. The luminosity distribution is broadly peaked on the arcjet centerline and diminishes smoothly within one diameter distance radially and about two diameters distance axially of the exit orifice. There is no luminous evidence of flow structure in the downstream exhaust until the background pressure (of helium) is increased to above several torr.

In the vicinity of 50-100 torr (helium background), jet structures are very apparent and closely resemble computer code predictions for the middle range of Mach numbers and density ratios ($M \approx 3 - 6$, $\eta = 0.1 - 0.3$). Figure 8 provides four black-and-white photos from a sequence recorded by the rotating mirror framing camera of a test in which an argon jet at a choked-flow rate of 8 g/s penetrates into a helium background of 100 torr. The current and voltage for this operation are provided in Figures 3 and 4. In the original photos, and with computer enhancement of the black-and-white images, four main features of the luminosity distribution are readily discerned. A bright (highly exposed) region at the nose of the jet displays the concave, and occasionally tre-foil, structure depicted in the computer code contour images. This structure propagates as a high luminosity region as the jet penetrates the target atmosphere by tens of exit orifice diameters. At the left side of the jet image the continued luminosity of the arcjet exit orifice is recorded, along with the apparent expansion of the exit flow. This expansion is turned axially downstream by the expected

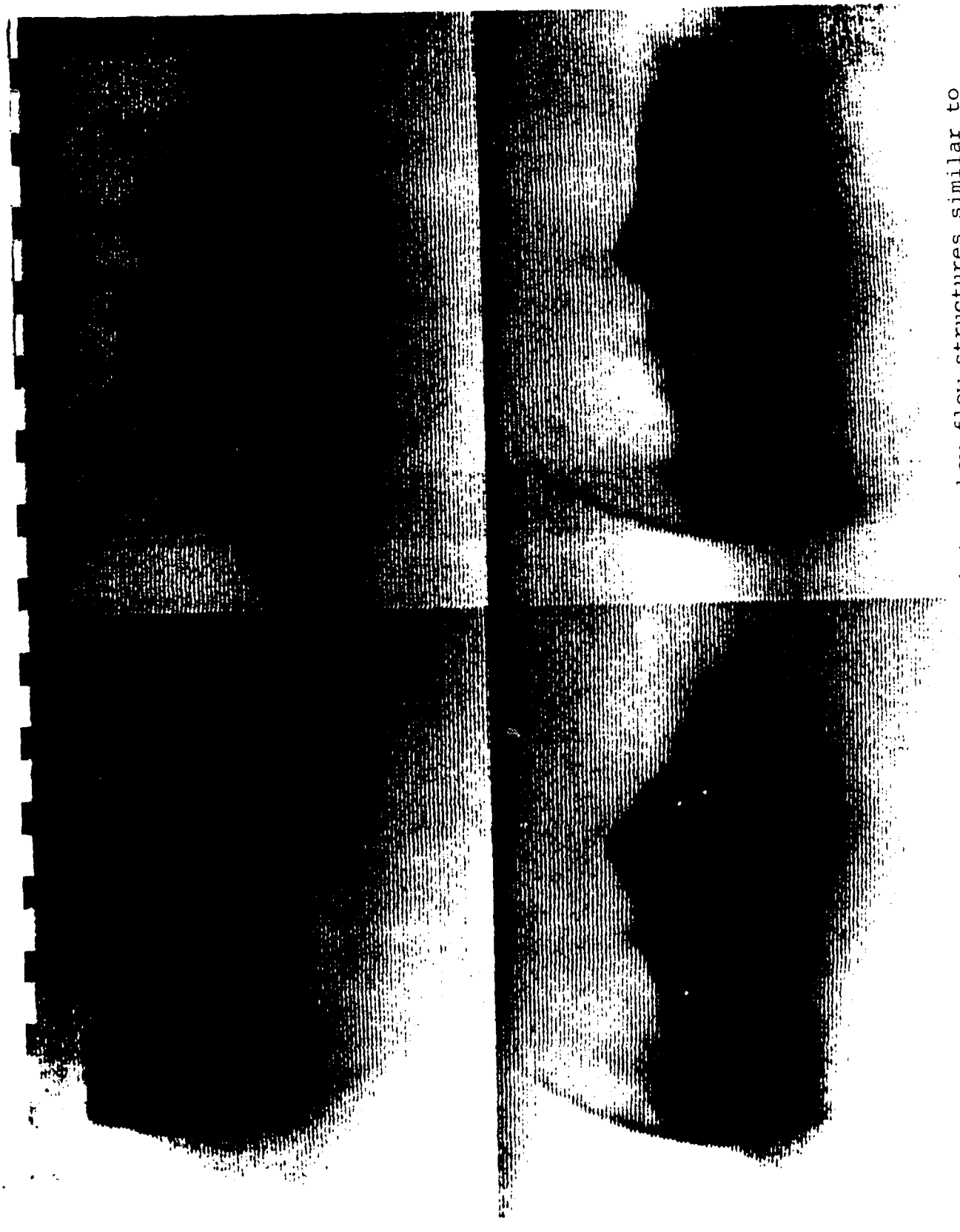

Figure 8. Time resolved black-and-white photos show flow structures similar to those envisioned by two-dimensional hydrocodes. Note the Mach disc indicating underexpanded flow from the plasmajet source and the concave nose of the propagating jet (seen also in the calculated images).

expansion waves reflecting from the jet centerline. Reflection of these waves at the free boundary of the jet as compression waves then results in a Mach disc normal to the jet centerline, as observed about three or four orifice diameters downstream of the exit. The medium level of luminosity of the jet core (between the high luminosity regions of the exit, Mach disc, and jet nose) is surrounded by a much lower luminosity region that displays a rather diffuse structure, resembling the so-called "cocoon" in the computer code predictions.

The black-and-white experimental images have been computer enhanced and colorized in relation to exposure intensity in order to emphasize flow structures. The same four frames in Figure 8 are repeated in Figure 9 and also on a larger format sequentially in Figures 10-13. (While colorization based simply on luminosity level retains some aspects of the flow structure, fine details that are readily discerned from the black-and-white images in terms of patterns of local gradients in luminosity tend to disappear. Additional work on image processing is probably warranted.) Figure 14 is a late time exposure from the same test and shows the long time persistence of the jet at its original diameter. The exit orifice and Mach disc region are still evident, but the jet nose is downstream of the field of view. (The larger radial extent of low intensity light near the right hand side appears to be photographic aberration on the original record.) Figures 15 and 16 provide the trajectory and derived velocity of the jet nose, based on the actual data film strip.

By placing a wedge in the downstream jet, the flow Mach number can be measured and the jet speed (vs the penetration speed) may be estimated. From a time-integrated photograph (Figure 17), the Mach number downstream of the Mach disc is $M = 2.5 \pm 0.4$, with imprecisions due to measurement of the shock angle and allowing a range of possible values of specific heat ratio from $\gamma = 1.3 - 1.6$, for argon at 0.5 to 2 eV. The associated range of jet flow speeds is then 2600 to 8000 m/s.

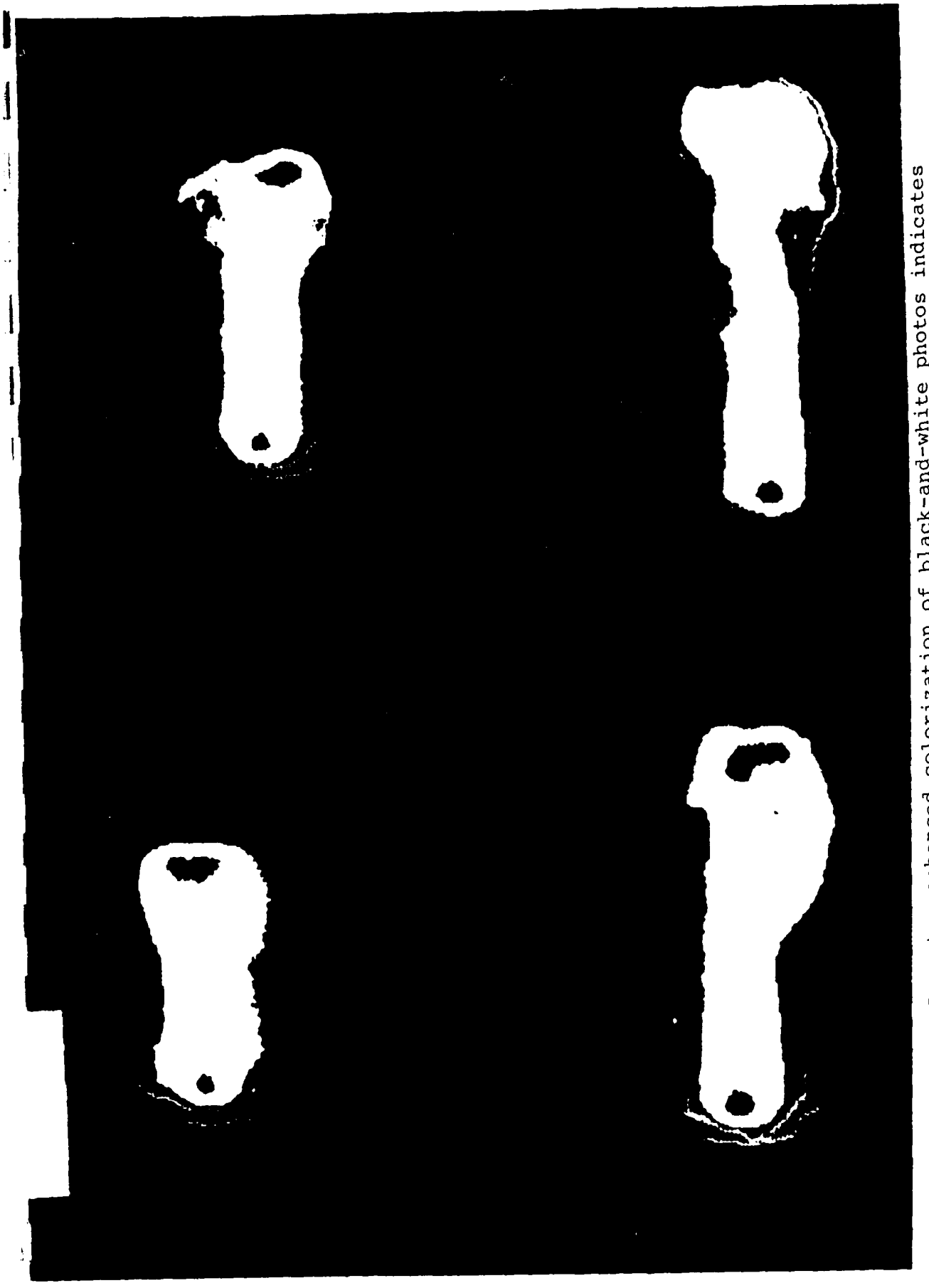

Figure 9. Computer enhanced colorization of black-and-white photos indicates region of exposure variation, but obscures fine scale structures seen on original balck-and-white photos.

Figure 10. Computer enhanced view of argon dense plasmajet propagation in 100 torr helium for 1.6 μs exposure 144 μs after current start.

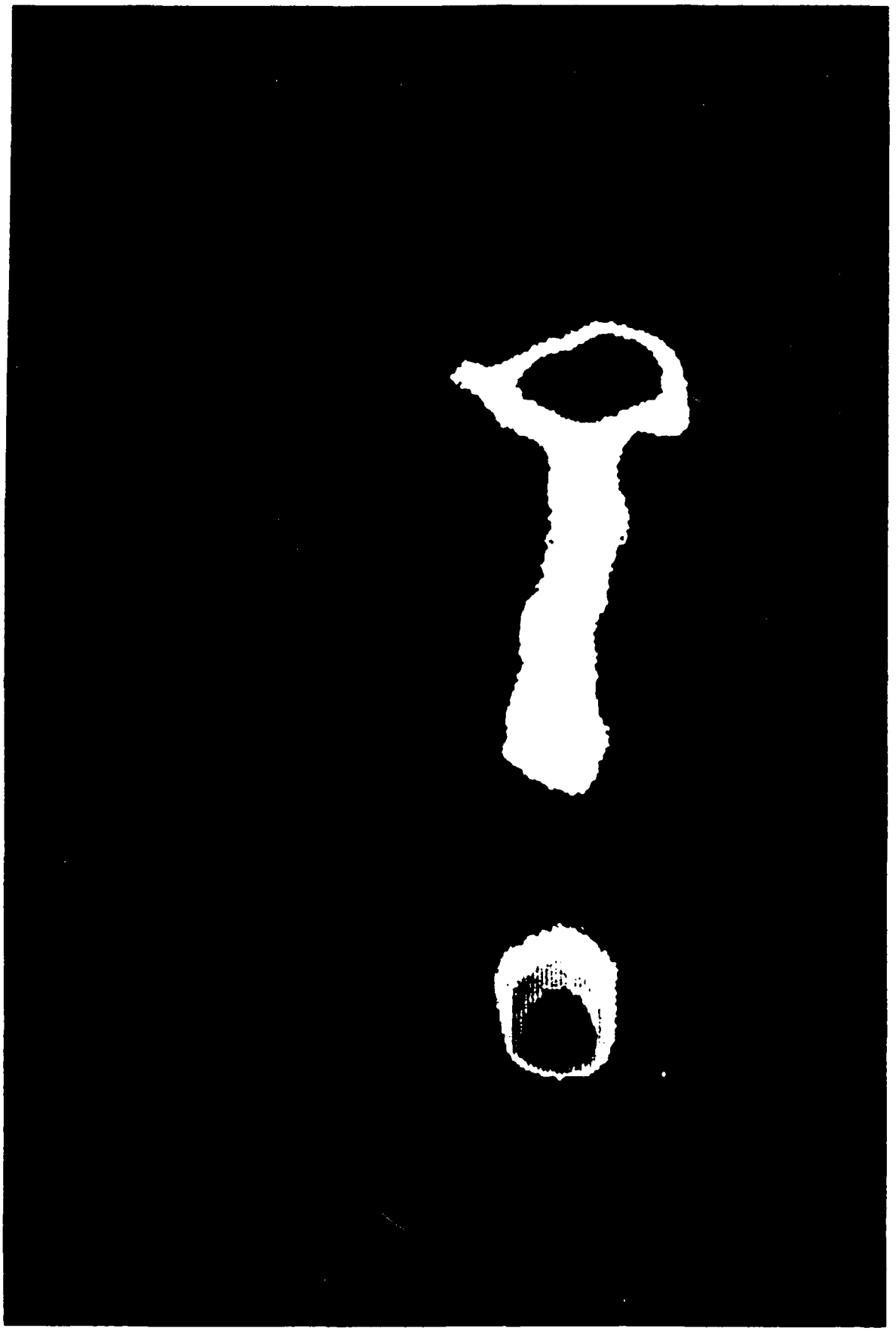

Figure 11. Computer enhanced view of argon dense plasmajet propagation in 100 torr helium for 1.6 μs exposure 170 μs after current start.

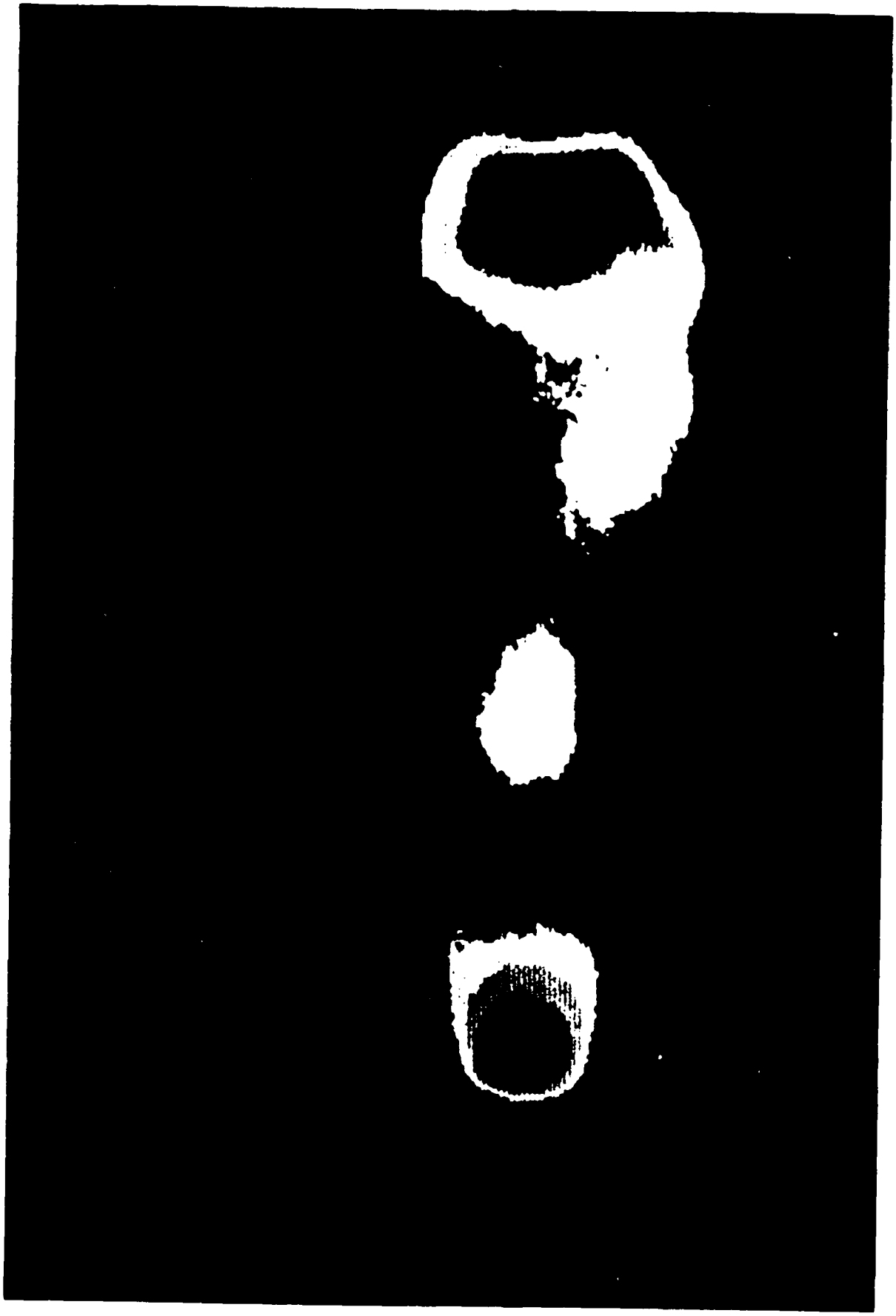

Figure 12. Computer enhanced view of argon dense plasmajet propagation in 100 torr helium for 1.6 μs exposure 196 μs after current start.

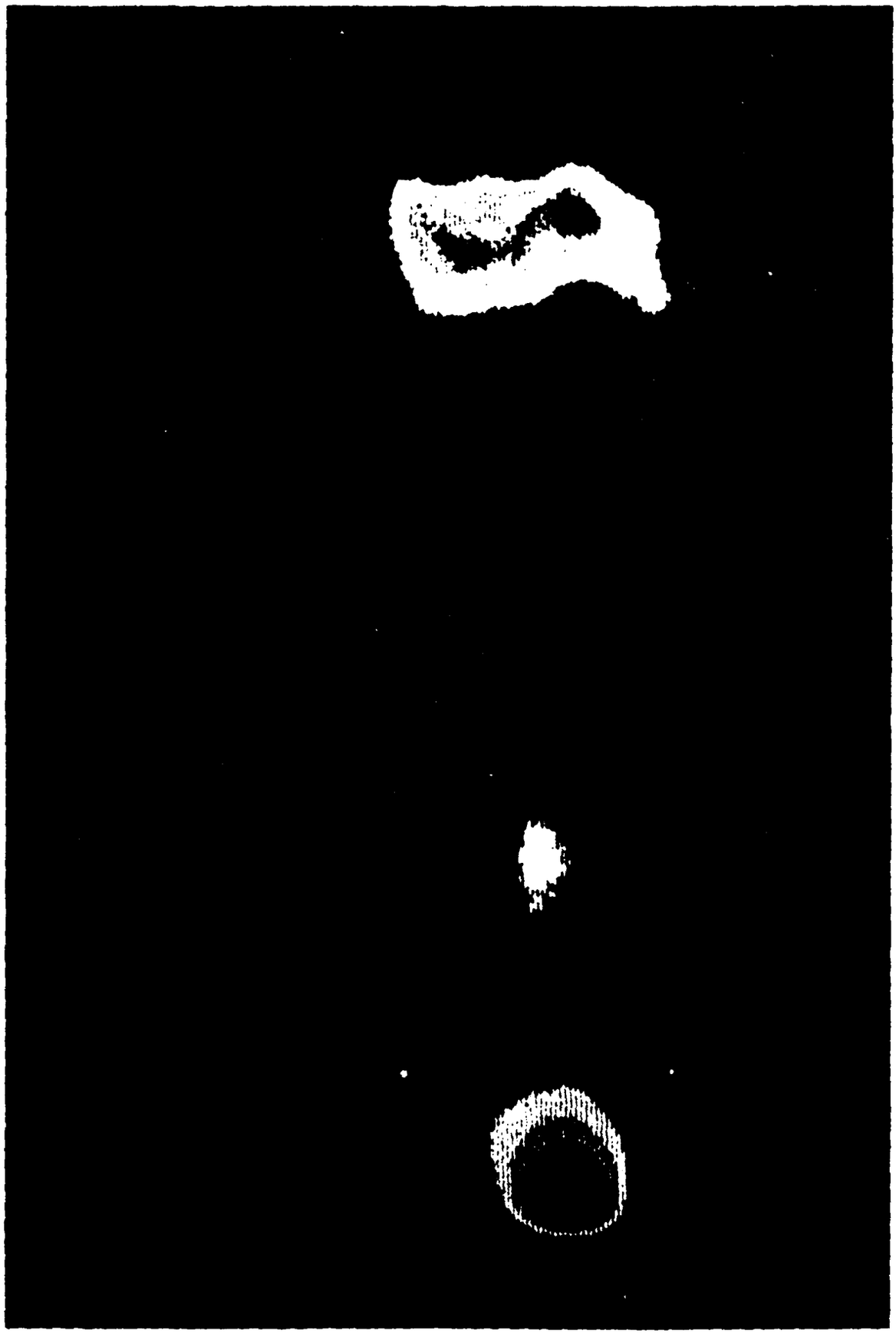

Figure 13. Computer enhanced view of argon dense plasmajet propagation in 100 torr helium from 1.6 μs exposure 223 μs after current start.

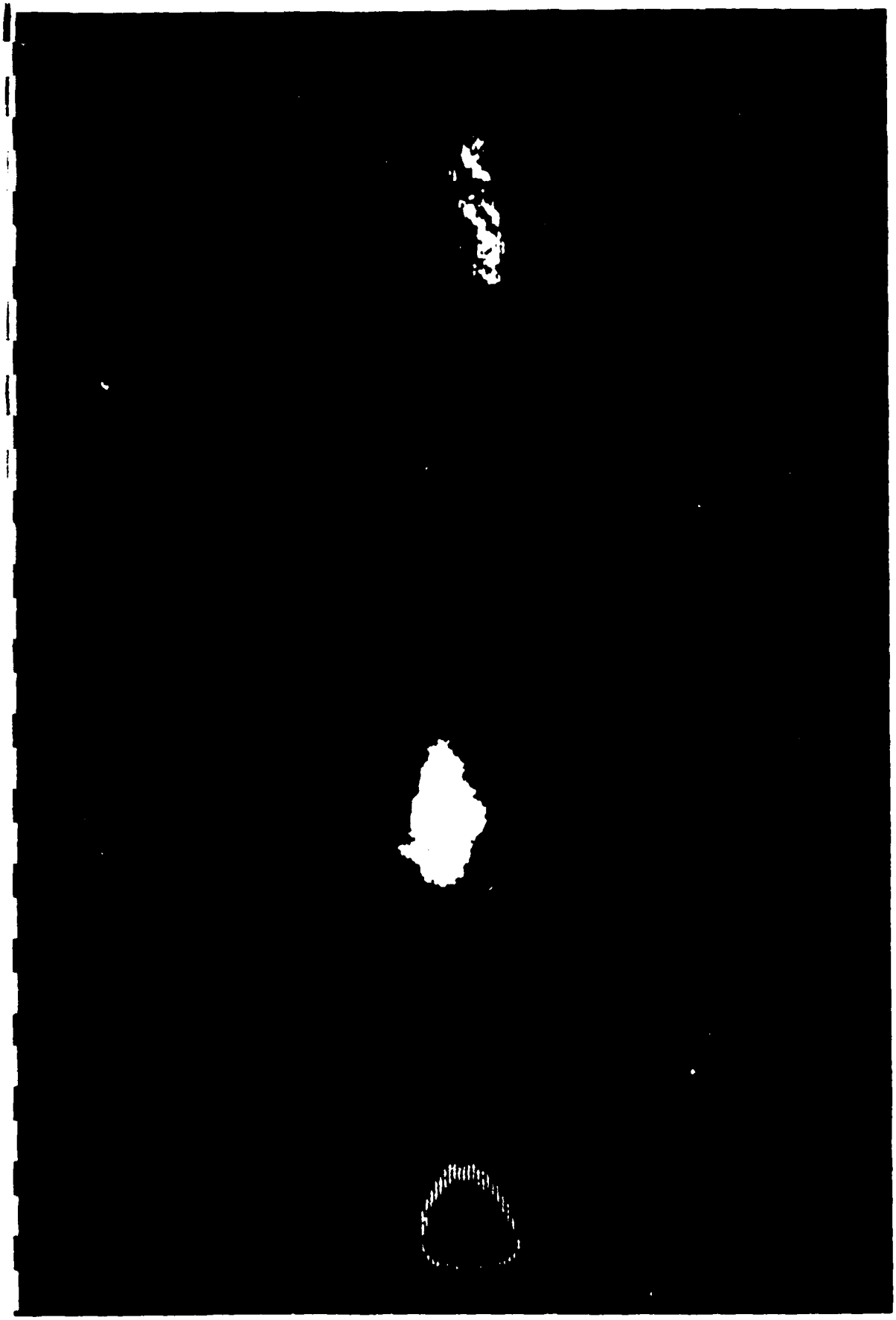

Figure 14. Computer enhanced view of argon dense plasmajet propagation in 100 torr helium for 1.6 μs exposure 355 μs after current start. (Nose of propagating jet is well downstream of present field of view).

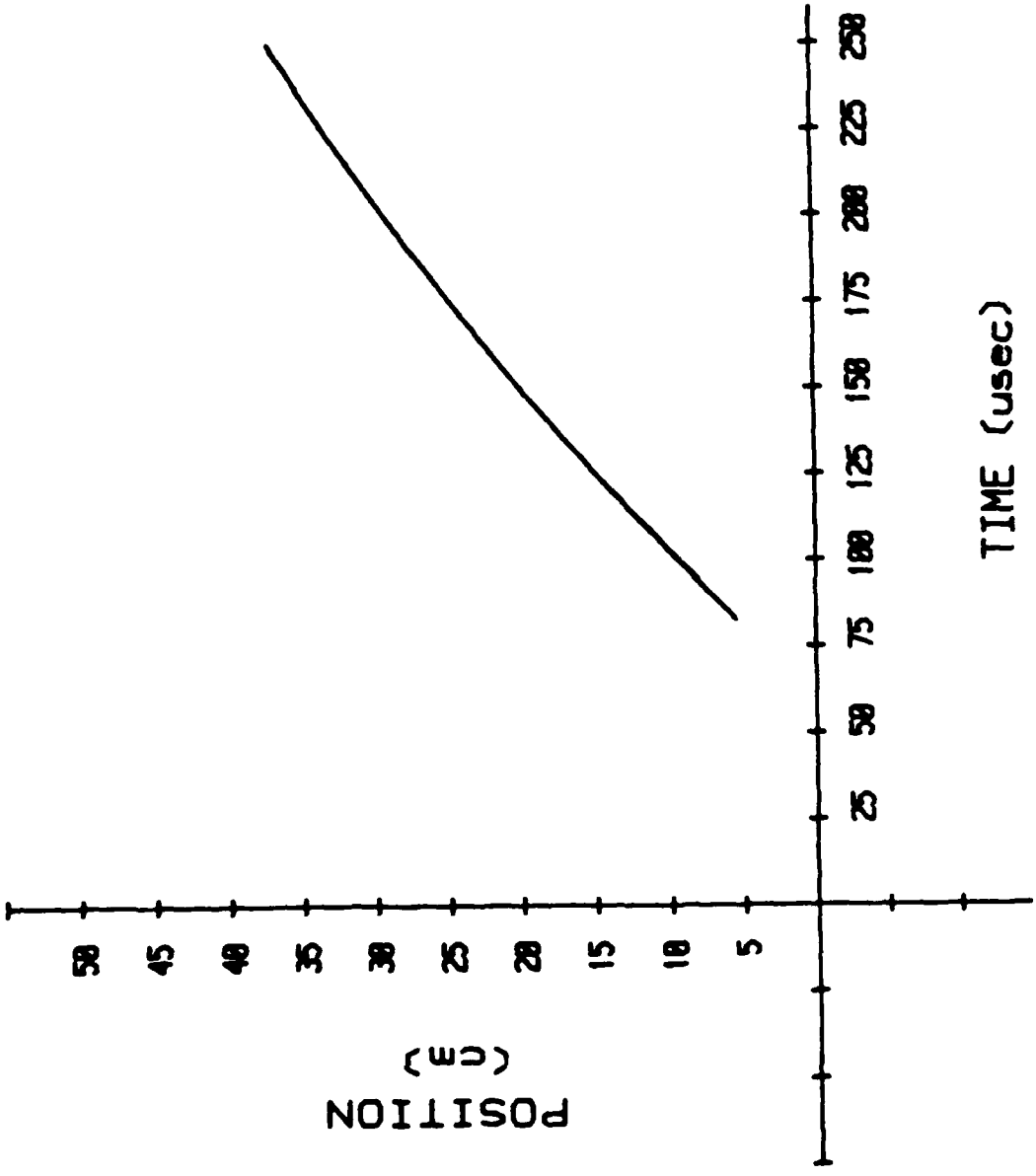

Figure 15. Jet penetration vs time for initial experiments for argon jet into 100 torr helium atmosphere from rotating mirror framing camera photos.

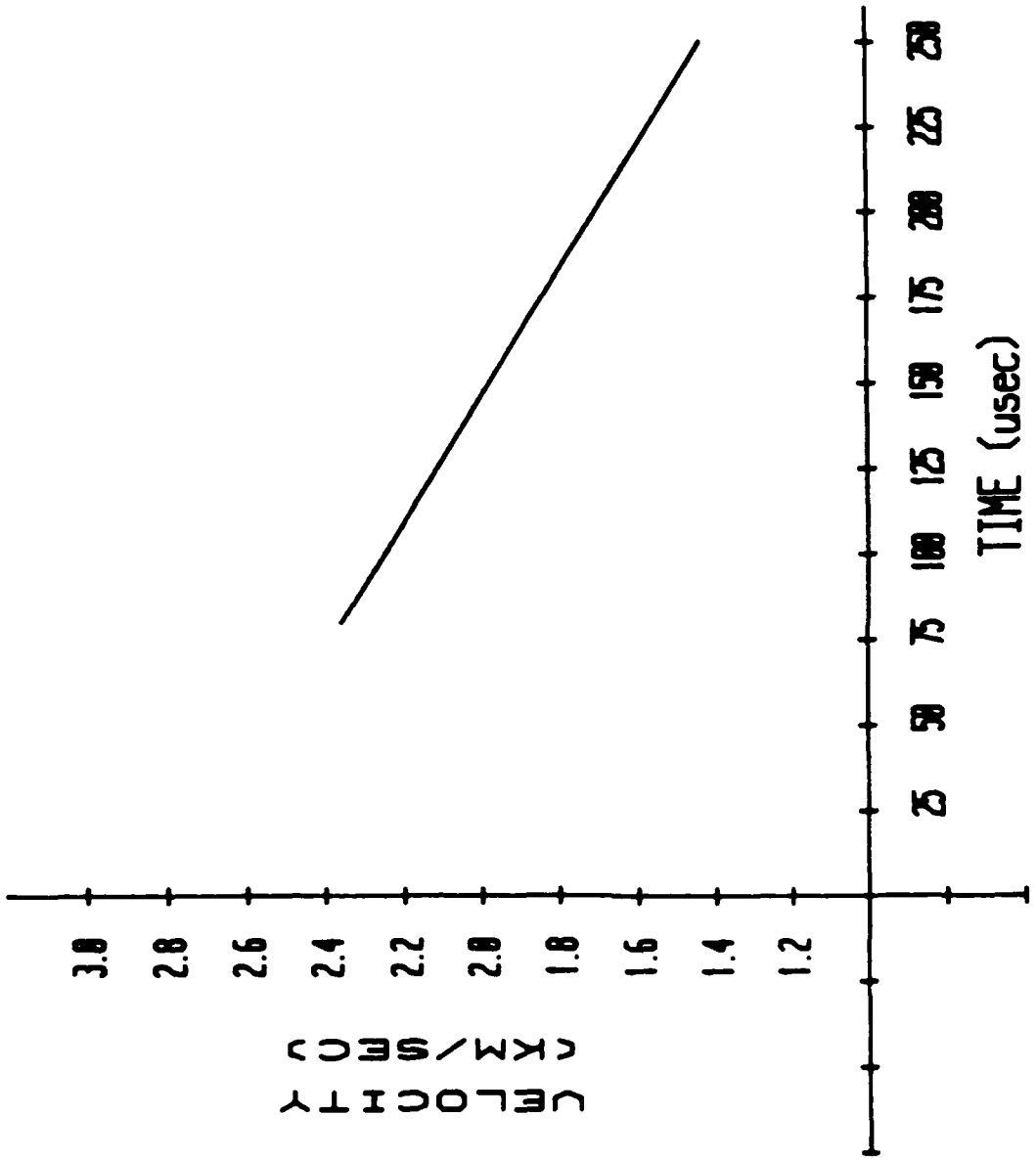

Figure 16. Jet penetration velocity vs time for initial experiments of argon jet into 100 torr helium atmosphere from data fit to position vs time of Figure 15.

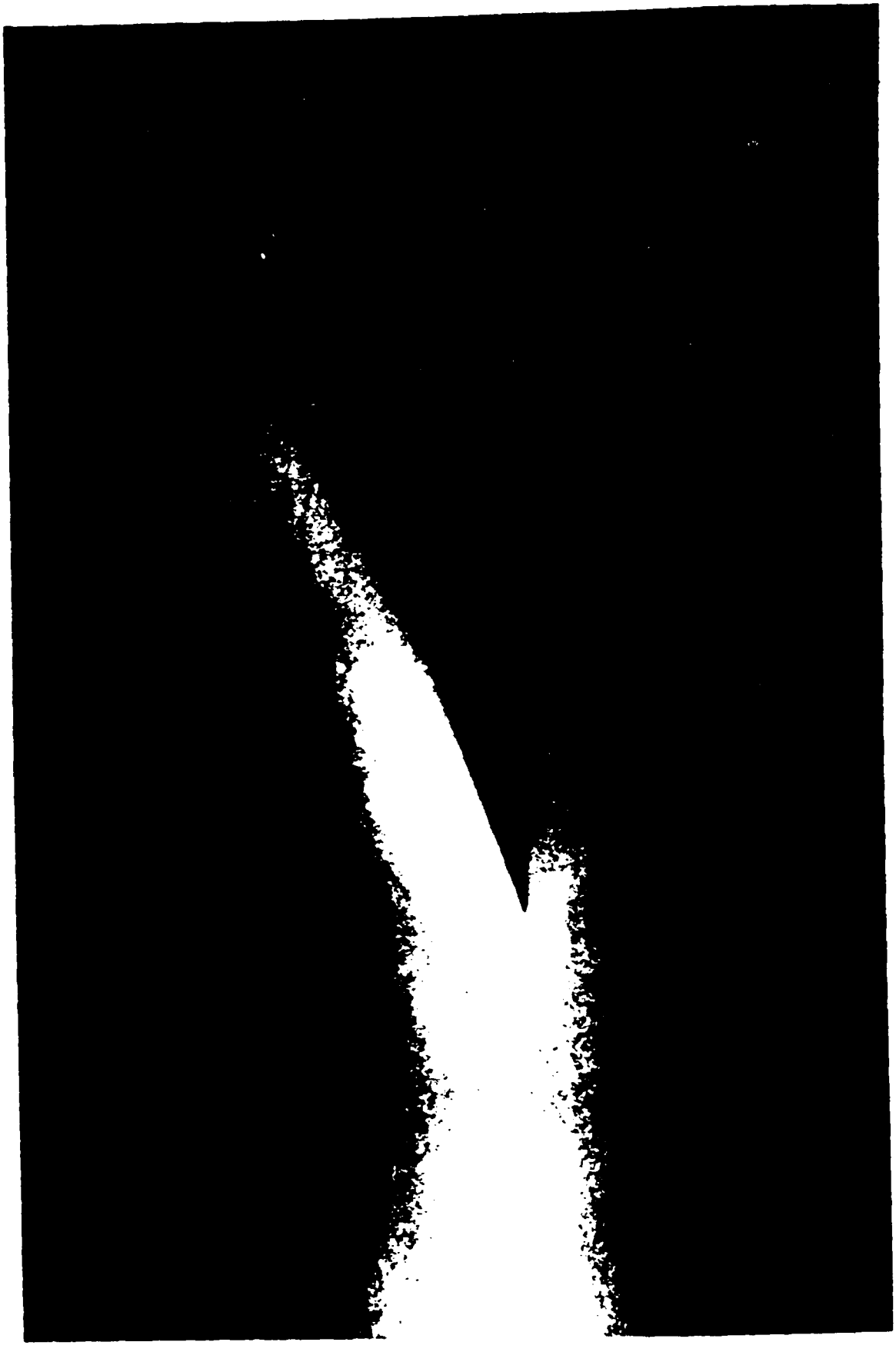

Figure 17. Time integrated photo of flow over a wedge indicates a Mach number downstream of the Mach disc of 2.5 ± 0.4 in reasonable agreement with jet propagation velocity from rotating mirror framing camera photos (u = 2000 m/s) and sound speed estimates for argon at a few electron volts.

Three separate factors contribute to the difficulty in using the wedge data and simple models. The first problem is due to the use of a time-integrated photograph. Some uncertainty in measurement of the shock angle is introduced by the early and late time flow interactions with the wedge (even though these have relatively short durations). Time-resolved photography will remove this uncertainty. A second problem involves the real behavior of a high speed, partially ionized flow with a cold surface (that might rapidly heat locally to provide ablation); analysis of shock angle informatic based on simple flows with constant specific heat ratio may be inadequate even for time-resolved measurements. The third and most basic problem in achieving consistency with gross measurements of detailed quantities is due to flow nonuniformities (expected from the numerical calculations), which immediately introduce inaccuracies in discussing the values of flow speed, density and temperature on the scale of jet dimensions. If the structure of the flow near the jet nose is ignored, then one-dimensional formulations can provide consistent values of flow properties at finite Mach numbers by matching stagnation pressures (Appendix I). Two-dimensional calculations, however, are necessary to obtain a self-consistent velocity distribution and nose structure. Estimates of the two-dimensional flow might be made in the same manner as hypersonic-blunt body flow analysis, but are not readily perfcrmed in the context of the free vortex ring structure near the jet nose.

For a jet penetration speed of 2000 m/s, and a Mach number based on the wedge photo of 2.5, the analysis in Appendix I provides a calculated jet temperature of 13 eV (with $\gamma = 1.4$) and the jet flow speed is 16.7 km/s. Use of the higher value of Mach number (within error bars) of 2.9, however, predicts a jet temperature of 2.4 eV and a flow speed of 8.3 km/s. While the values obtained are not unreasonable, it is useful to improve experimental conditions both in terms of t'e arcjet source and diagnostic techniques.

VI. EXPERIMENTS WITH MODIFIED ARCJET SOURCE

A portion of the difficulties involved in the interpretation of the initial experimental results derived from the existence of a Mach disc a few diameters downstream of the exit orifice. This disc-like flow structure is due to compression waves from the free boundary of the jet that resulted from expansion waves and their reflections generated to match the pressure and velocity of the jet as it enters the lower pressure background atmosphere. With a constant bore exit channel, the electrically-heated argon flow can leave the arcjet in an under-expanded state. Addition of a nozzle, in principle, allows this flow to expand within solid boundaries, converting internal energy to directed kinetic energy without flow nonuniformities. The Mach number of the jet thereby improves due to both the increase in exhaust speed and decrease in temperature.

To maintain the exit dimensions of the jet (3 cm diam), a nozzle region was added by creation of a throat (1 cm diam) about 2 cm downstream of the end of the cathode (center-conductor), as shown in Figure 18. Higher thermal loadings were anticipated on the cathode tip and in the throat so these portions of the arcjet were machined from a tungsten-copper alloy (Elkonite). The dimensions and shape of the channel were established with the aim of maintaining arcjet current patterns within the thrust chamber by allowing flow expansion through a minimum area orifice in the arcjet anode. (The details of an actual arcjet flow including heat addition and viscosity are quite complex and have not been considered here because of the demands of time and resources at this stage in the program. After sufficient success has been achieved in creating high speed jet propagation, there may be resource levels available for calculational support of arcjet design.) The current and voltage characteristics of the modified arcjet are essentially the same as previously (Figures 3-5), so the basic discharge conditions within the thrust chamber have probably not changed significantly with inclusion of the nozzle.

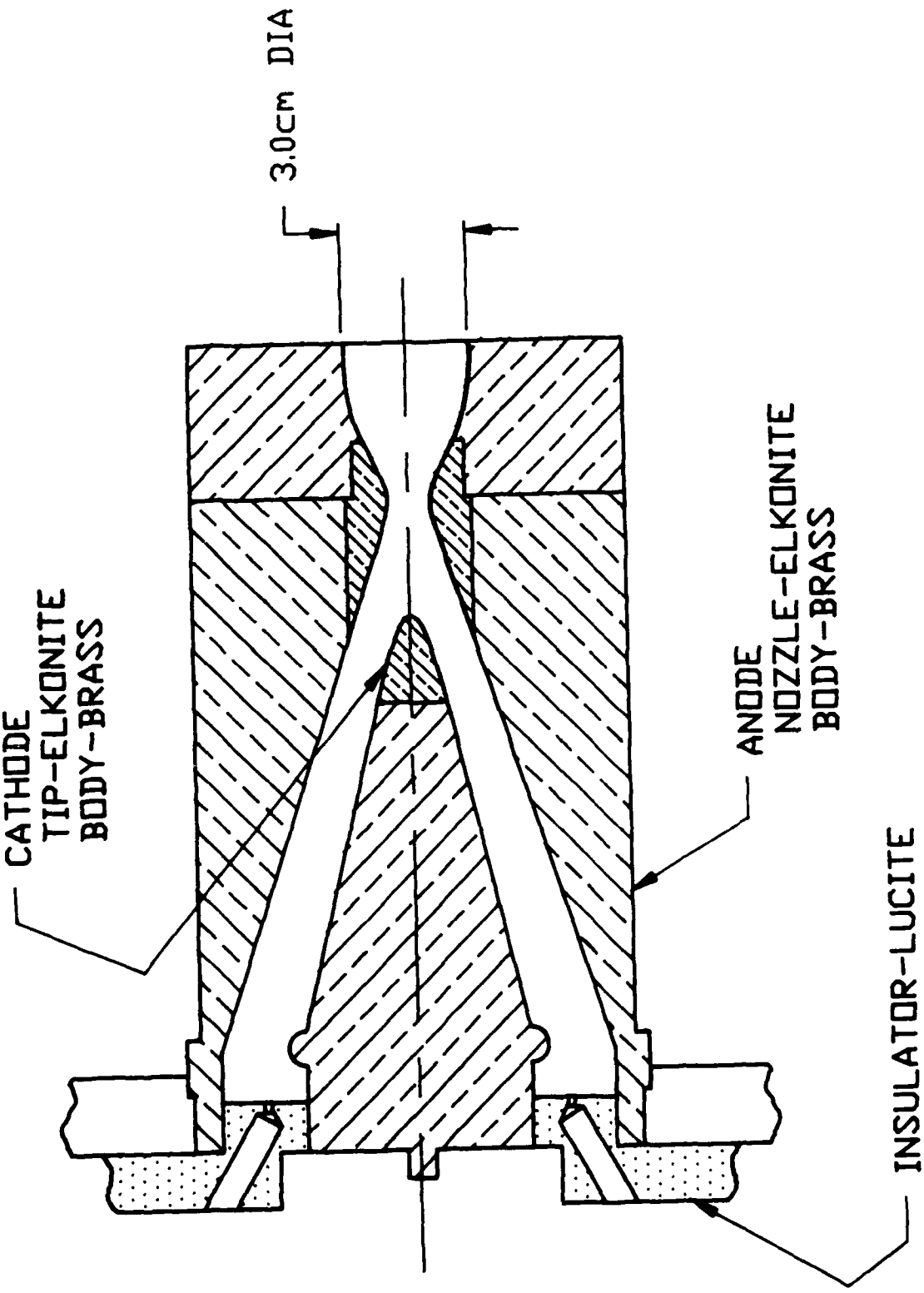

Figure 18. Schematic of arcjet source modified by addition of a nozzle downstream of the cathode.

The jet flow appears to have improved substantially, however, as indicated by the sharper and more axially-directed jet boundary at the exit. The basic flow is displayed in Figure 19, which is a time-integrated photograph of the jet interacting with a wedge. (Note that the view is directed slightly upstream to look at the exit orifice.) In the original photographs, viewing directly across the wedge surface, the shock interaction with the free jet boundary is observed, including a reduction in the luminosity behind the oblique shock by expansion waves from the boundary and their reflections off the wedge surface. Compression waves generated at the free boundary by these reflected expansion waves then create a second luminous shock when they converge and reflect at the wedge surface. The Mach number of the flow is 3.2 - 4.8, (for γ = 1.3 - 1.67) which is considerably higher than achieved with the initial arcjet source. The flow also appears to be cooler simply based on the color of the exhaust (less blue, more pink) and also on the lack of luminous states beyond argon I.

Figures 20 and 21 display the trajectory of the jet penetration and the derived penetration speed for an argon jet directed into helium. The argon choked-flow rate is again set for 8 g/s and the helium fill pressure is 75 torr. The average penetration speed is about the same as for the initial arcjet experiments (but increases rather than decreases slightly with time). Flow structures near the nose of the jet (shown in Figure 22) again closely resemble the numerically predicted shapes and there is again a low intensity surrounding cocoon. Optical photography using the rotating-mirror framing camera permits direct color images to be obtained. Figure 23 displays color photos of a jet under the same conditions as Figure 22. In Figure 24, the jet associated with a lower mass flow rate is displayed. This result was obtained by operating with the arcjet plenum filled by the initial helium pre-fill (i.e., no argon input). Basic flow structures are again visible, but the overall penetration is faster (2200 m/s vs 1800 m/s, average penetration speed). This result suggests that the window of stable propagation is not very

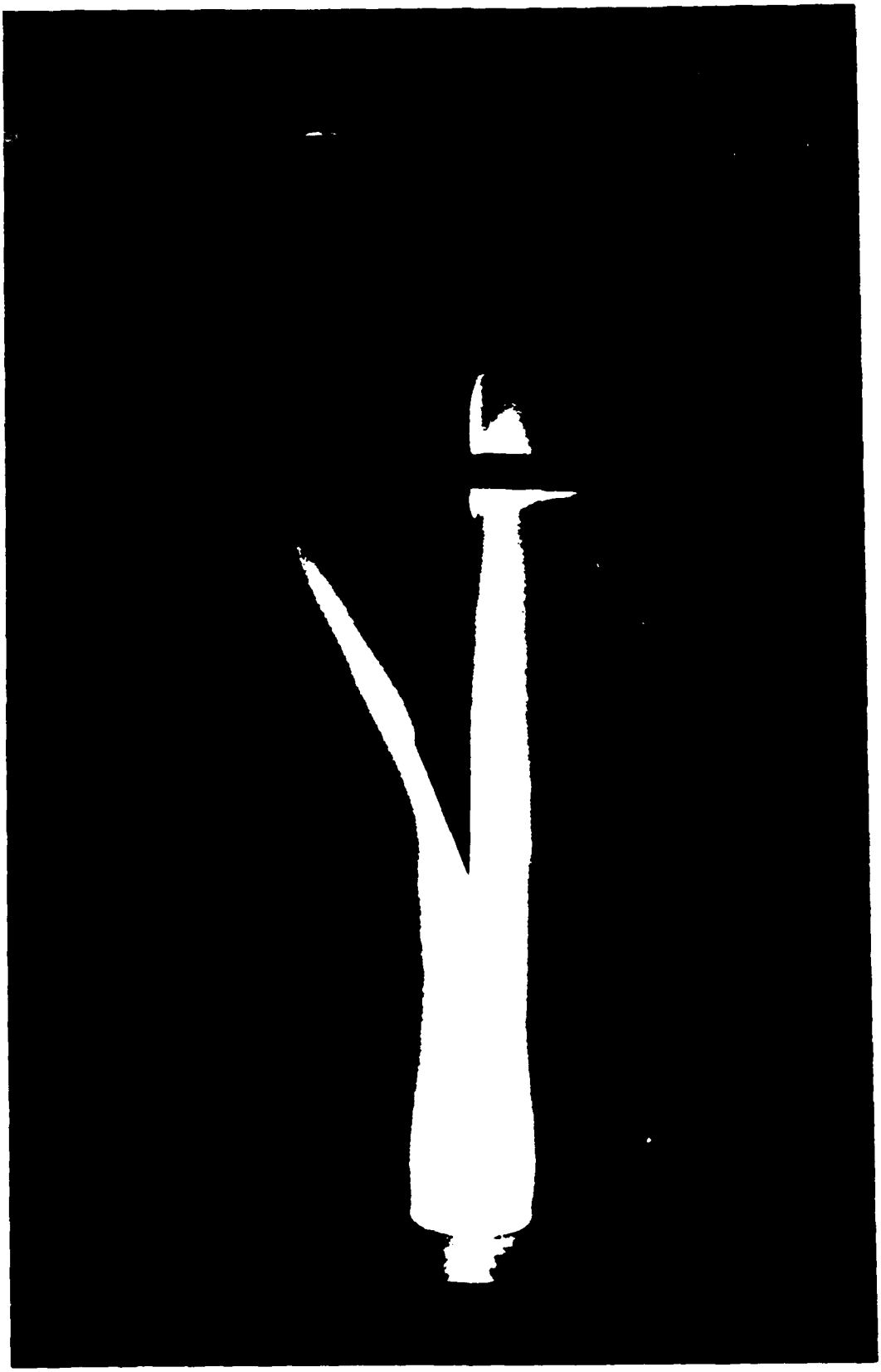

Figure 19. Time integrated photo of flow over wedge with modified arcjet source indicates a Mach number of 4.0 ± 0.8 in reasonable agreement with jet propagation velocity from rotating mirror framing camera photos and sound speed estimates for argon at approximately 1 eV.

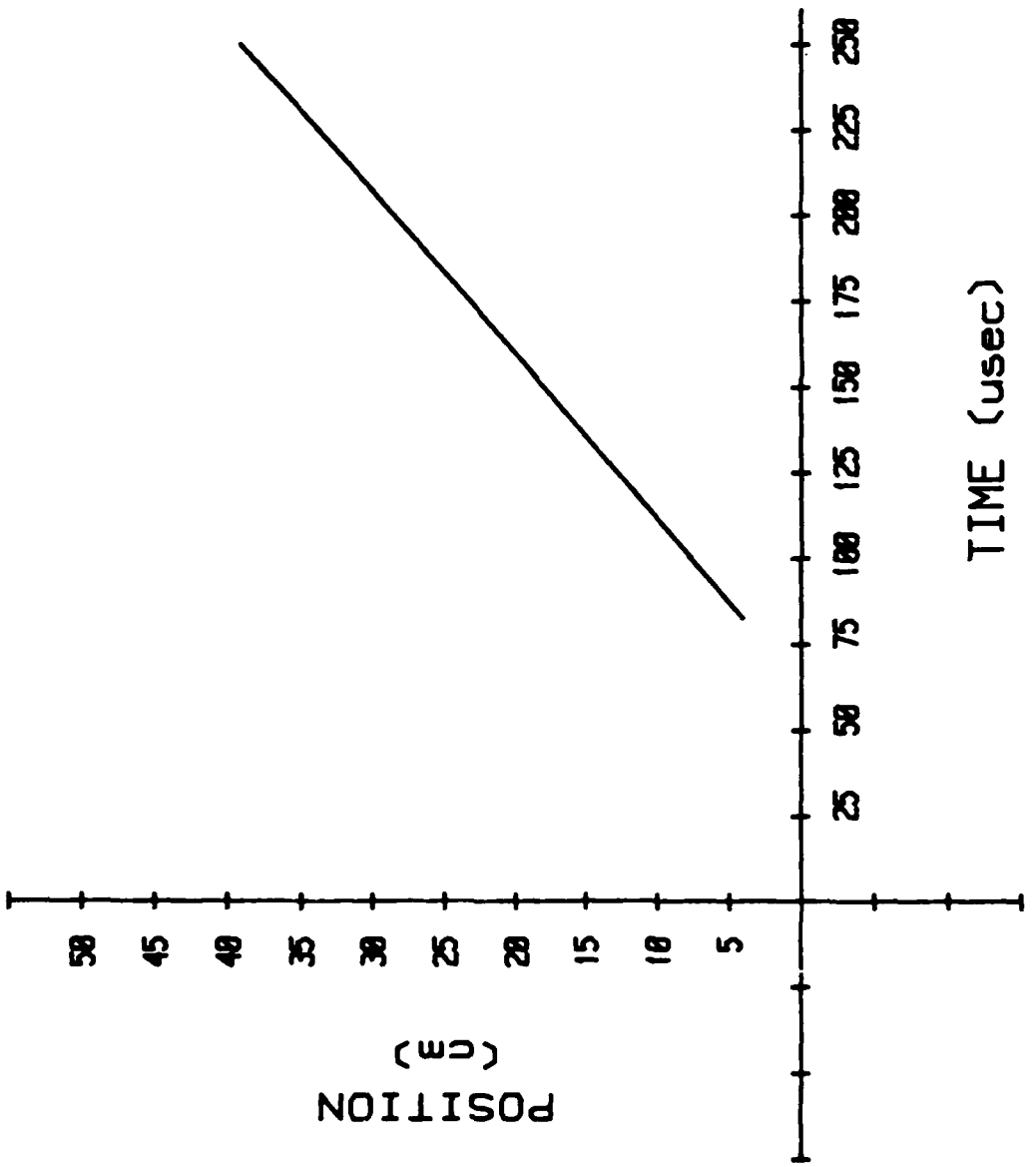

Figure 20. Jet penetration vs time for argon jet into 75 torr helium atmosphere using modified arcjet source.

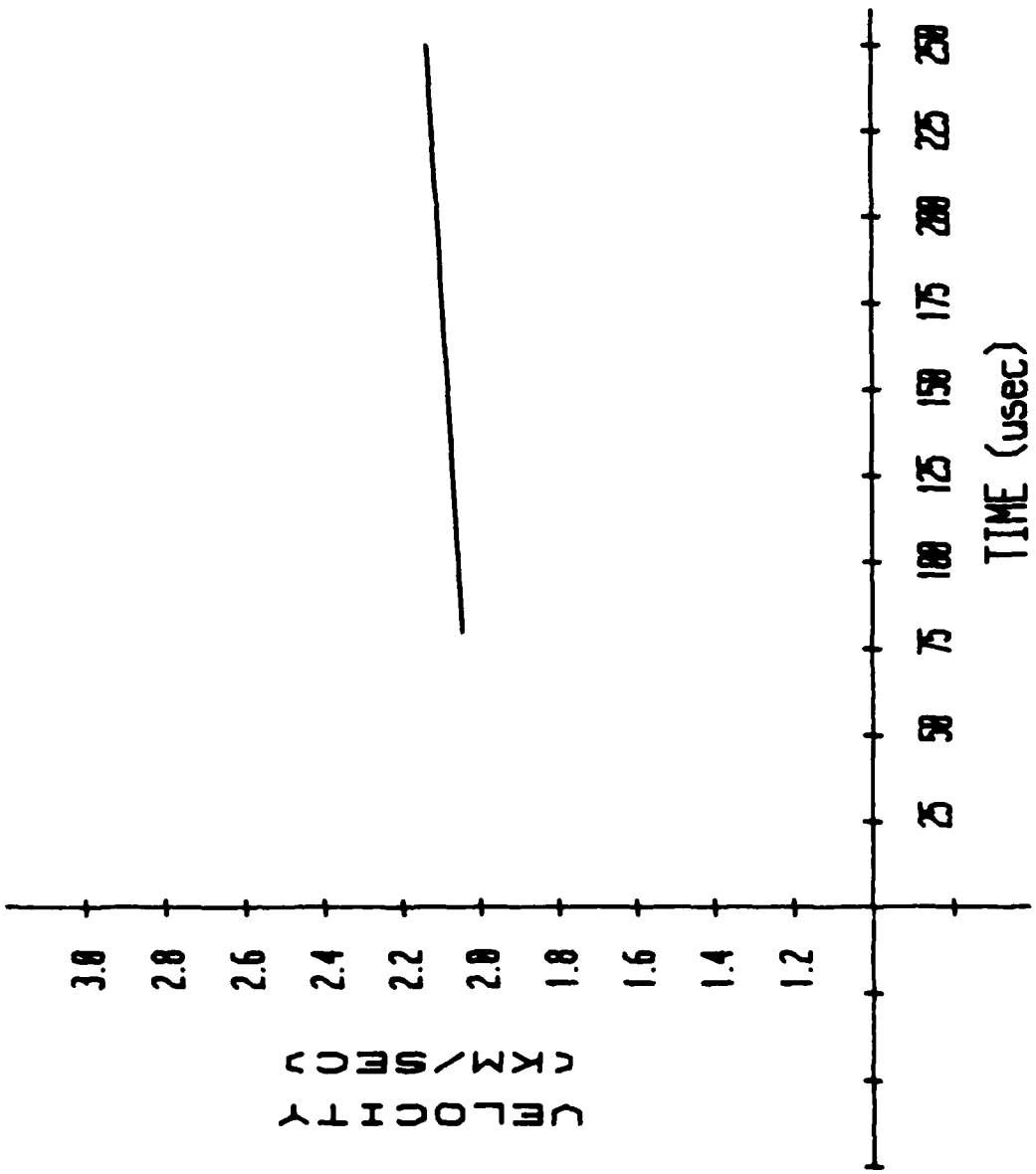

Figure 21. Penetration velocity vs time for argon jet into 75 torr helium atmosphere fit to position vs time of Figure 20.

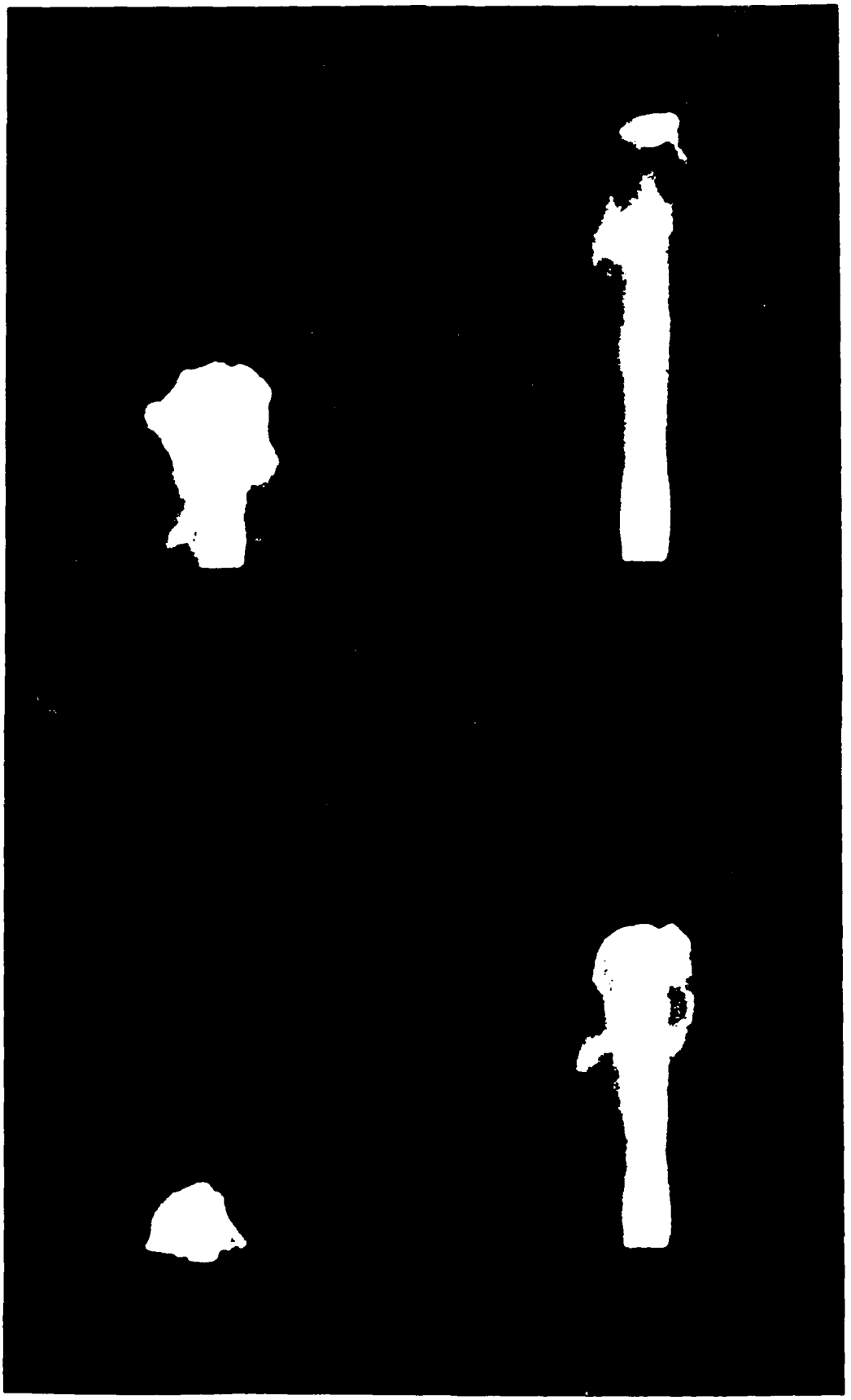

Figure 22. Rotating mirror framing camera black-and-white photos of argon jet into 75 torr helium atmosphere with modified arcjet source. Each frame exposure is 3.82 μs with frames 1,2,3,&4 at 88, 118.4, 148.8 and 189.4 μs, respectively, after current start.

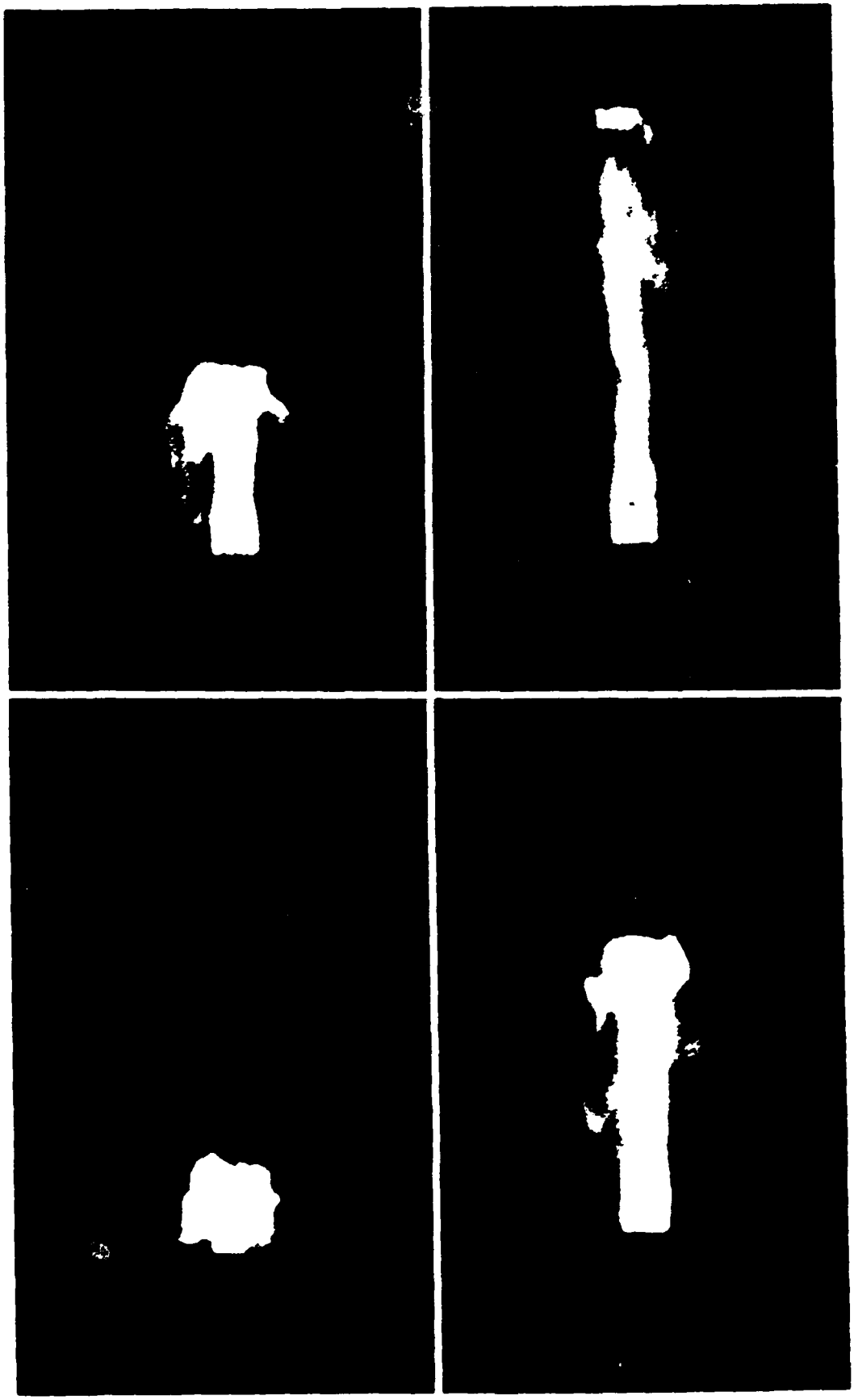

Figure 23. Color photos of argon jet propagating into 75 torr helium atmosphere using modified arcjet source. Direct color images are obtained with a rotating mirror framing camera and color film.

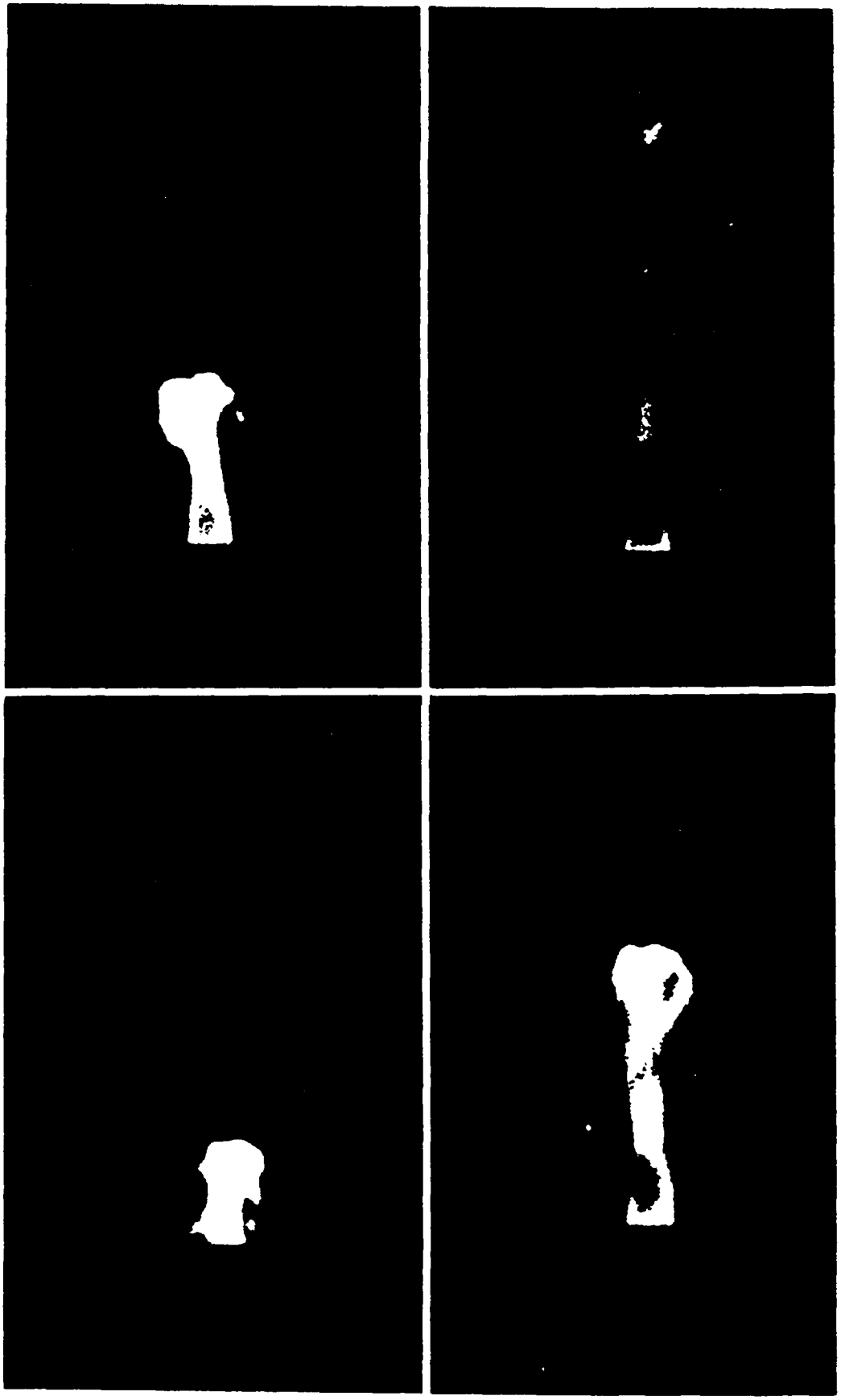

Figure 24. Color photos of helium jet propagating into 75 torr helium atmosphere.

narrow (including equal molecular weights for jet and atmosphere, and factors of almost two in mass flow rate).

Application of the analysis in Appendix I to the experimental measurements with the modified arcjet flow using argon provide values of jet temperature and flow speed of 0.7 eV and 5300 m/s, respectively, for an assumed specific heat ratio $\gamma_J = 1.4$, and a penetration speed of 2000 m/s. The calculated temperature is consistent with the lack of luminous states above argon I and corresponds to a (total) plasma density of 9×10^{22} m^{-3}. This density is consistent with electron density estimates of 2×10^{22} m^{-3} at the exit orifice plane from the width of the H_α line associated with trace amounts of hydrogen provided in the arcjet flow. The density ratio η of the propagating jet for these conditions is about 0.28, so, with $M \approx 4$, the present experiment is operating in a regime well below that for mode-dominated instability and outside the less well-defined region of cocoon-dominated flow (see Figure 2).

At the calculated density, the mass flow rate would be 17 g/s vs 8 g/s for the choked-flow rate. There is little spectroscopic evidence of significant contribution by ablation to the arcjet flow. Usually, quasi-steady MPD arcjets are operated into vacuum with choked-flow at the injectors. In the present experiments, however, the initial argon pressure in the arcjet chamber due to the downstream pressure of the helium target atmosphere may be sufficient to supply the mass flow for the duration of present current pulse.

As a separate (but related) check on consistency, it is possible to pose the computations in a form for which the arithmetic is easier than in Appendix I. Since the jet penetration speed into the radially-confining atmosphere and the jet diameter appear to be nearly constant, it is reasonable to apply the simple momentum equation analysis (Appendix I) in order to relate jet properties. In particular, the mass flow rate is:

$$\dot{m} = \rho_J u_J A_J$$

$$= \rho_a u_p A_J \, \eta \left(1 + \frac{1}{\eta^{1/2}}\right)$$

so the mass density ratio η may be estimated from quantities that in principle are available experimentally. The equation for η is:

$$\eta + \eta^{1/2} - \frac{\dot{m}}{\rho_a u_p A_J} = 0$$

from which,

$$\eta = \left[\frac{(1 + 4\dot{m}/\rho_a u_p A_J)^{1/2} - 1}{2}\right]^2 .$$

For $\dot{m}$ = 8 g/s, u_p = 2100 m/s, A_J = 7.07 cm^2 and a background atmosphere of helium at 75 torr (ρ_a = 1.66 x 10^{-2} kg/m^3), the mass density ratio is η = 0.067. The jet speed is therefore $u_J = (1 + \eta^{-1/2})u_p = 4.88\ u_p$ = 10.2 km/s.

From the jet speed and the Mach number estimated using the time-integrated wedge flow photographs, the sound speed in the jet should be 2125 - 3188 m/s (for γ = 1.67 - 1.3). The momentum balance model assumes static pressure equilibrium ($p_a = p_J$) so

$$p_J = \rho_J R_J T_J$$

$$= \eta \rho_a R_J T_J = \rho_a R_a T_a \quad ,$$

where R is the effective gas constant for the jet and atmosphere, as indicated by subscripts. The sound speed is defined in the same terms, namely $c = \sqrt{\gamma RT}$, so the effective specific heat ratio for the jet may be computed and compared with assumed values to check consistency:

$$\gamma = \frac{c^2(\gamma)}{R_J T_J} \quad \frac{\eta c^2(\gamma)}{R_a T_a}$$

with $R_a T_a$ = 6.25 x 10^5 m^2/s^2 for helium at room temperature, γ = 1.1 (for assumed value γ = 1.3) and γ = 0.49 (for assumed value γ = 1.67). The lower assumed value of γ yields a more consistent value of specific heat ratio, suggesting that the higher sound speed estimate is more accurate. The resulting jet

temperature, however, would then be about 3.7 eV, for which some indication of argon II radiation would be expected.

If the mass flow rate is actually 17 g/s (due to thrust chamber filling prior to arc initiation), then the preceding computations provide a value of η = 0.23 and a jet flow speed of 6512 m/s. For M = 3.2 (γ = 1.3), the sound speed in the jet is 2035 m/s, which results in a computed value of specific heat ratio $\gamma = \eta c^2/R_a T_a$ = 1.5; a value for γ of 1.4 may therefore be appropriate. The jet temperature with γ = 1.4 is T_J = 1.2 eV. At this temperature, with η = 0.23, the heavy particle density is 5.6 x 10^{22} m^{-3}, while the total particle density to provide pressure balance P_a/kT_J = 5.1 x 10^{22} m^{-3}, suggesting, within the inaccuracies of the calculation, that the average degree of ionization is very low. Further work is clearly needed to determine the jet density in a manner that is not model dependent. In the next section, spectroscopic analysis is used to examine the penetrating jet flow in its self-luminosity. Additional design consideration is required in order to control the arcjet mass flow rate. The modified arcjet source, in fact, appears to operate as an electrothermal vs electromagnetic arcjet. The jet flow Mach number is completely consistent with a 9:1 area ratio expansion from a choked nozzle of a flow whose stagnation temperature is a few eV. Future arcjet sources will operate with high magnetic pressure levels (~ 100 atm vs 1 atm) in order to achieve jet penetration speeds > 10 km/s.

VII. SPECTROSCOPIC MEASUREMENTS OF DENSE PLASMA JET

A spectroscopic analysis of a dense plasma jet penetrating a radially-confining atmosphere has been performed using a digital spectral and spatial data acquisition system. The data system is comprised of a 1.2 meter f/11.5 spectrograph with an EG&G intensified optical multichannel analyzer (SIT camera) attached at the exit plane. The dense plasma jet and diagnostic system are shown schematically in Figure 25. The spectral and spatially resolved optical measurements were performed at 15 and 30 centimeters axially downstream of the orifice of the source in order to determine the local electron temperature and density.

For determination of the electron temperature, relative argon line intensities were measured, Abel-inverted to yield local emissivities and compared by assuming that excited state densities are determined by Boltzmann statistics (Boltzmann plot technique). Figure 26 shows the relative population of excited neutral argon at 15 cm from the source where (a) 2p levels at 13.299 eV; (b) 4d' levels at 14.753 eV. Figure 27 shows the relative population of excited neutral argon at 30 cm from the source where (a) 2p levels at 13.299 eV; (c) 3p levels at 14.506 eV. This analysis suggests that the relative excited argon populations are not correlated to an electron temperature and therefore in the jet they are determined by recombination rates into excited states and by radiative cascade. The true electron temperature is then relatively low with electron heating coming from only collisional de-excitation of excited states and from three body recombination.

Figures 26 and 27 indicate strong spatial features at the argon channel-helium interface region at the two axial locations. These figures, shown schematically in Figure 28 in relation to the arcjet (radial scale), indicate the development of three trends. In the central region of the channel the relative excited state densities decrease rapidly to values below detection limits with an increase in the observed hollow-shell

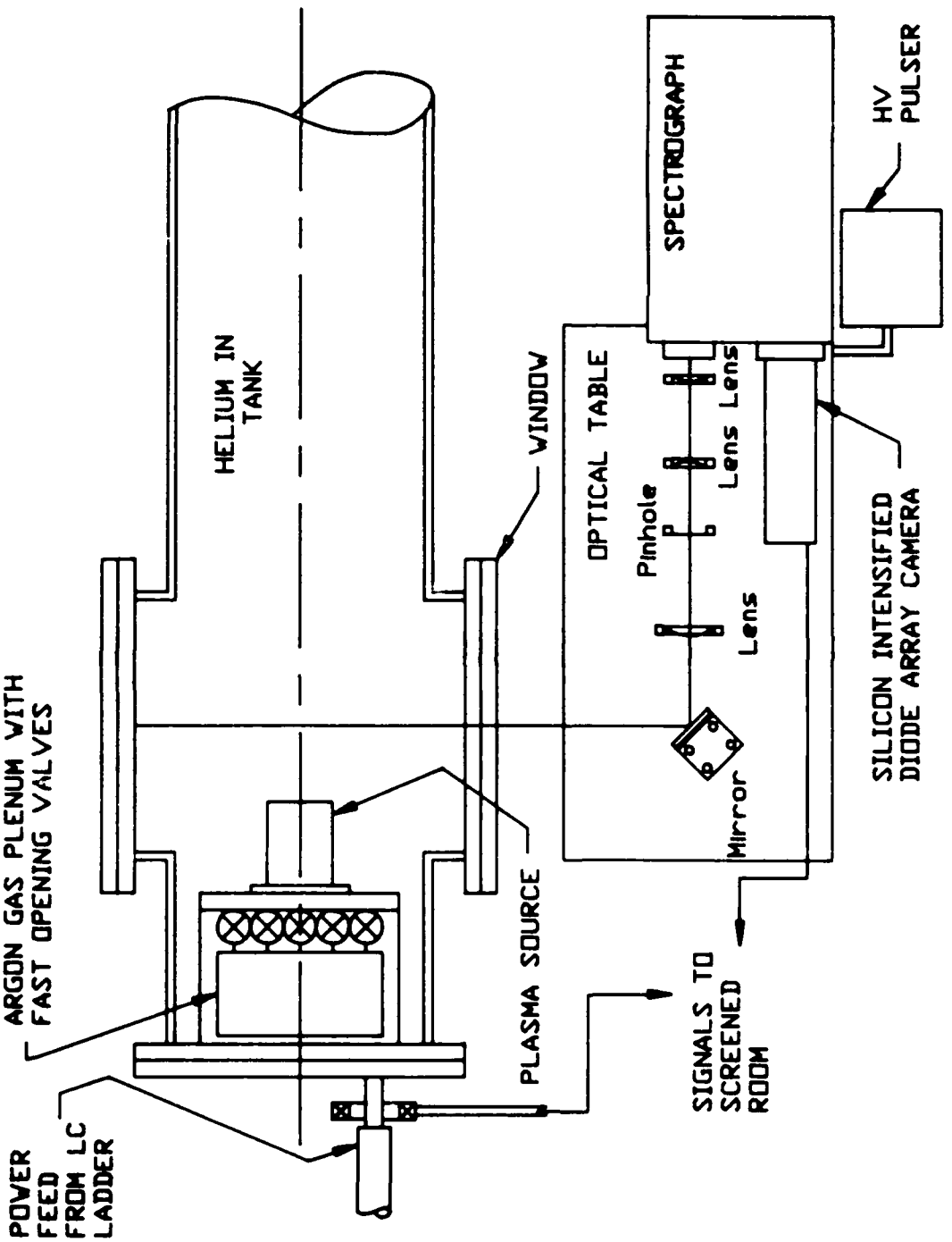

Figure 25. Schematic of experimental apparatus showing optical data acquisition system.

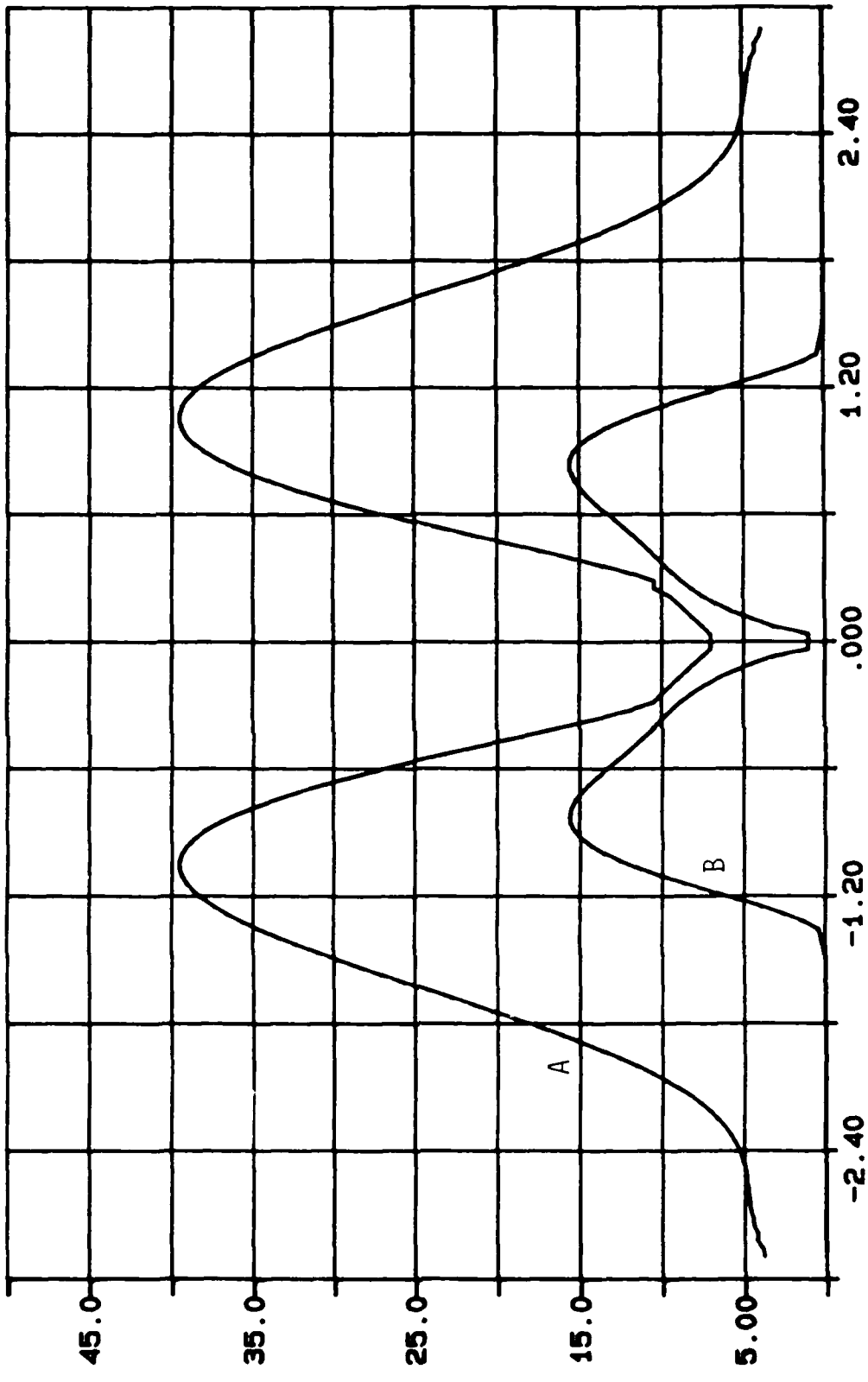

Figure 26. Relative population of neutral argon excited levels from observed line intensities at 15 cm from dense plasma jet source for (a) 2p levels at 13.299 eV; (b) 4d' levels at 14.753 eV.

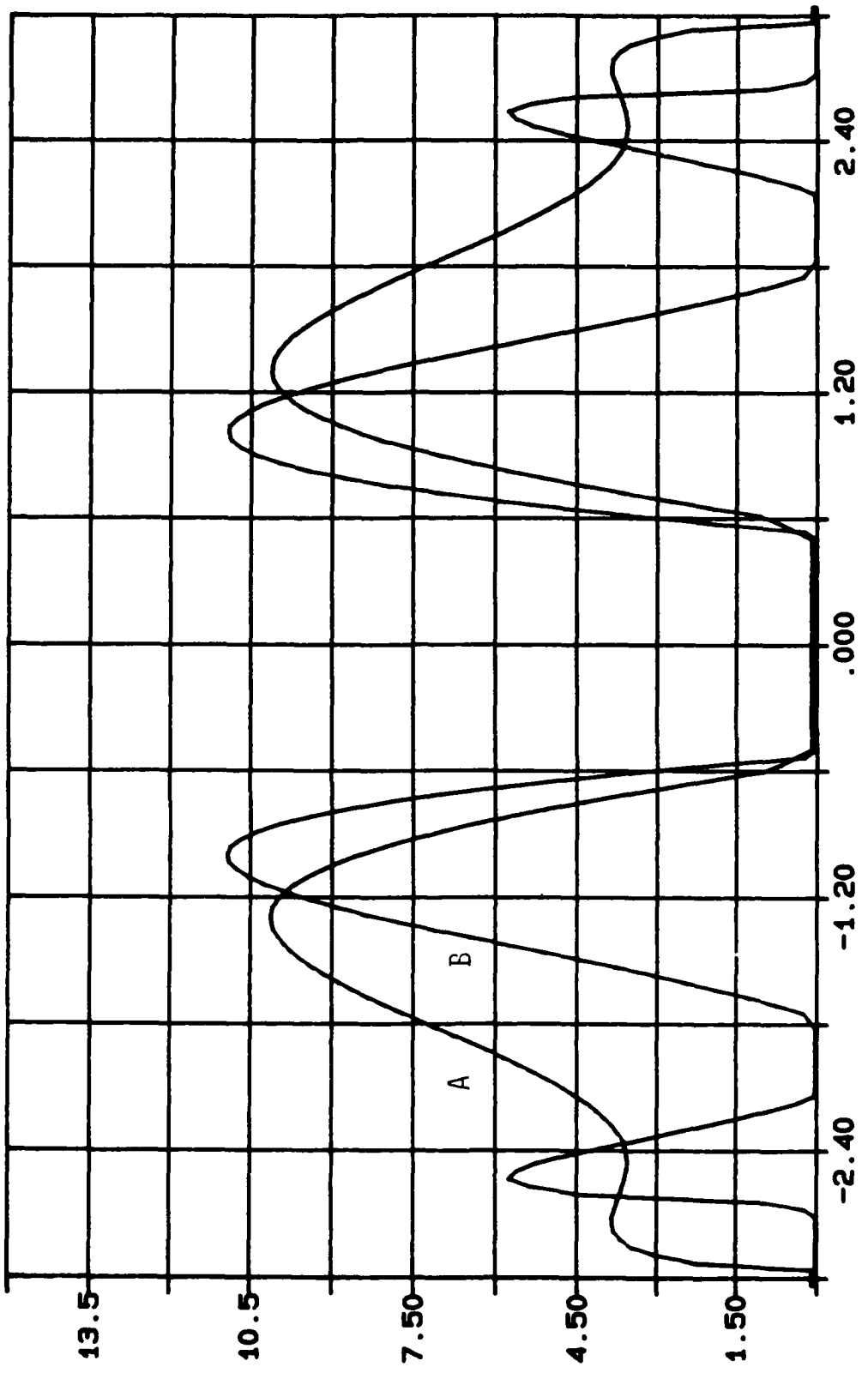

Figure 27. Relative population of neutral argon excited levels from observed line intensities at 30 cm from dense plasma jet source for (a) 2p levels at 13.299 eV; (b) 3p levels at 14.506 eV.

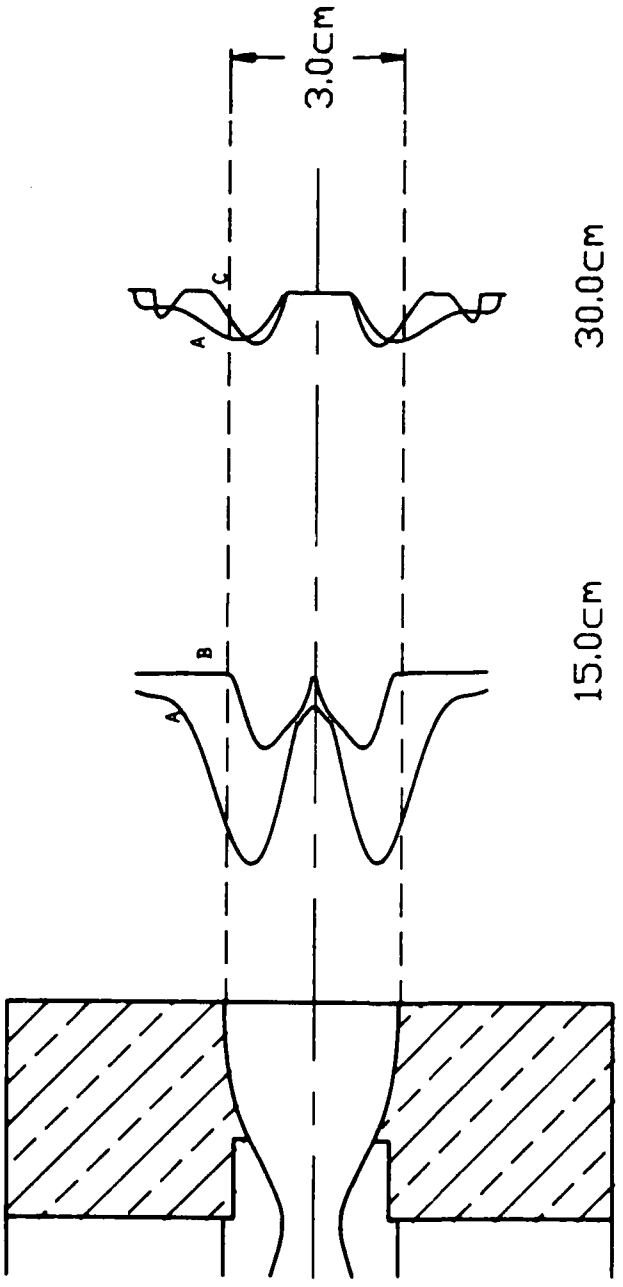

Figure 28. Relative population of neutral argon excited levels from observed line intensities at 15 cm and 30 cm indicates that the argon flow structure is preserved. [(a) 2p levels at 13.299 eV; (b) 4d' levels at 14.753 eV; (c) 3p levels at 14.506 eV.]

light intensity distribution. At the argon-helium interface region the argon intensities are decreasing but the argon flow structure appears to be preserved. External to the argon-helium interface region a second argon emission region seems to be developing (during the total exposure time of 200 μsec).

The measurement of Stark profiles permit the determination of the electron density independent of local argon excited state densities and with relaxed requirements for local thermodynamic equilibrium. For determination of the local electron density, the emission line profile must be measured both spatially and spectrally and then Abel-inverted to yield true local line profile. The measured line profile is then corrected for Doppler and instrument broadening and fit to a Lorentzian profile to yield spatially-resolved electron density. Figure 29 shows electron density versus radius at 15 cm as determined from line profile measurement of 503.213 nm Ar I. Figure 30 shows electron density versus radius at 30 cm as determined from H_α emission. These figures, shown schematically in Figure 31 in relation to the arcjet, show structures similar to argon emission shown in Figure 28. At 30 cm downstream of the source the observed electron density profile is more hollow than would be concluded from figure 28. The annular thickness of the electron density at 30 cm is approximately 6 mm whereas at 15 cm downstream of the source the observed electron density profile is on the order of 10 mm. Note also that the nominal shell diameter is preserved at approximately 2.5 - 2.7 cm between 15 and 30 cm downstream of the source with spatial instrument error of $\pm$ 0.2 cm.

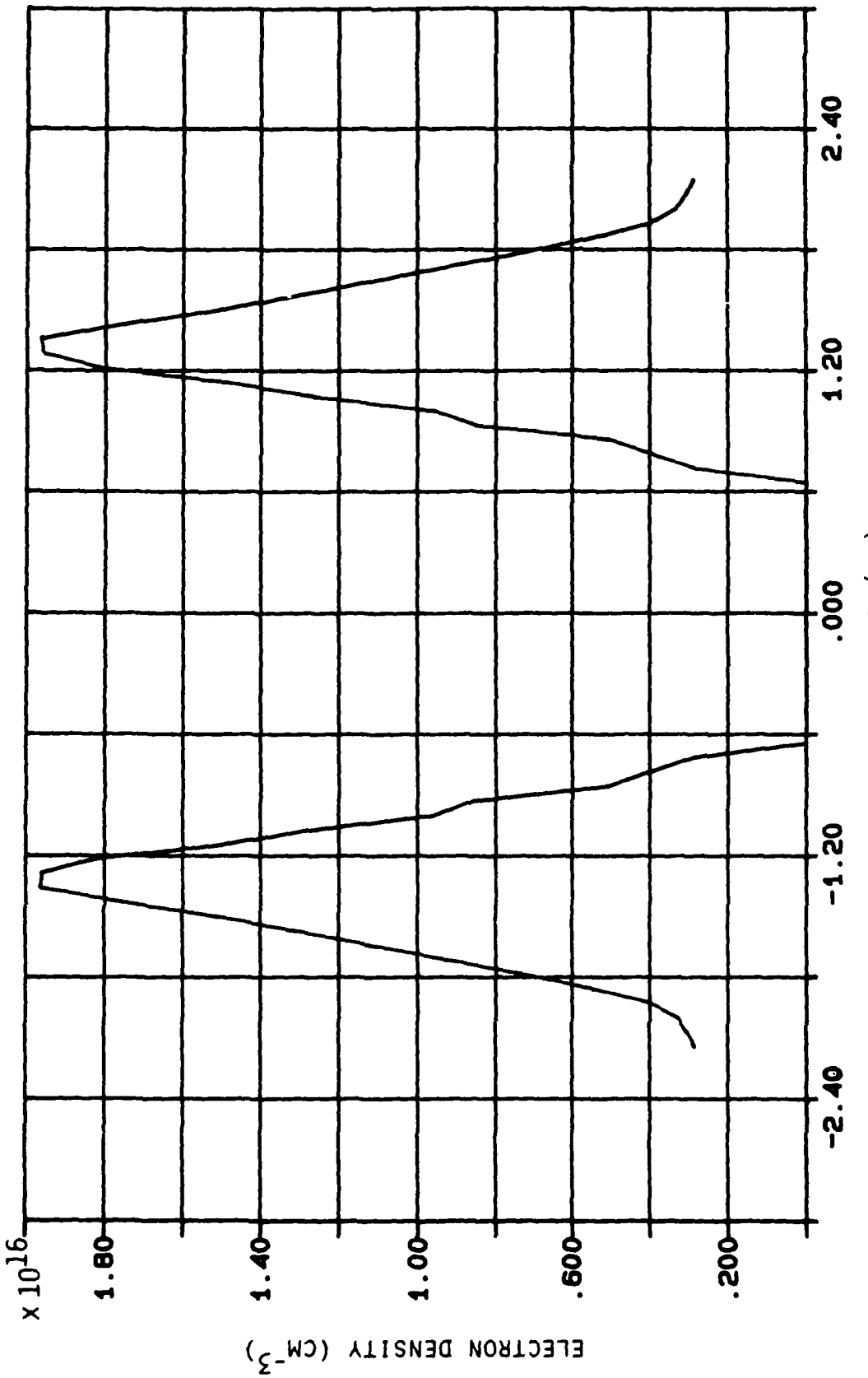

Figure 29. Electron density profile versus radius at 15 cm from dense plasma jet source from Stark width measurements of 603.213 nm argon I emission.

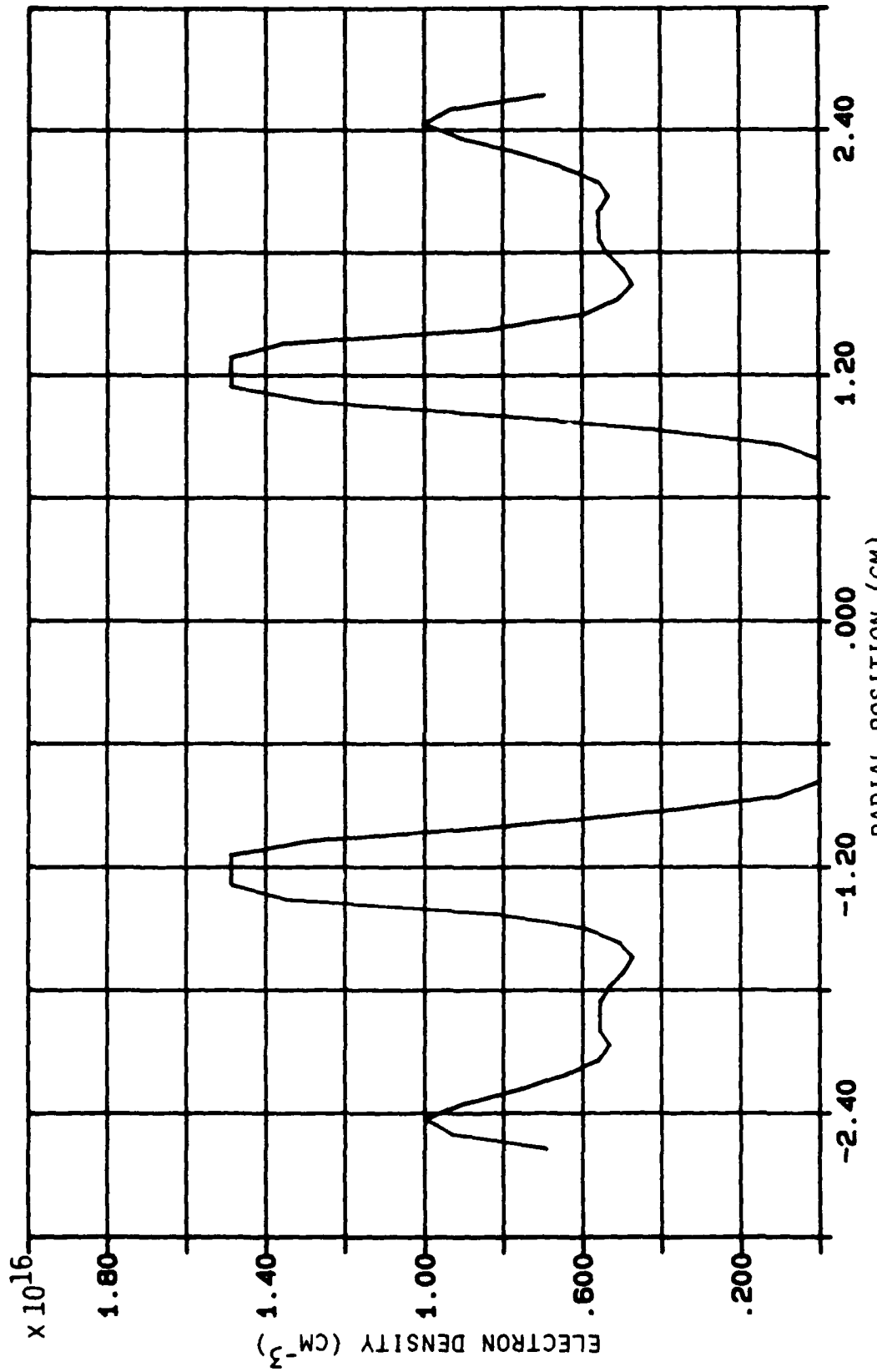

Figure 30. Electron density profile versus radius at 30 cm from dense plasma jet source from Stark width measurements of H_α emission.

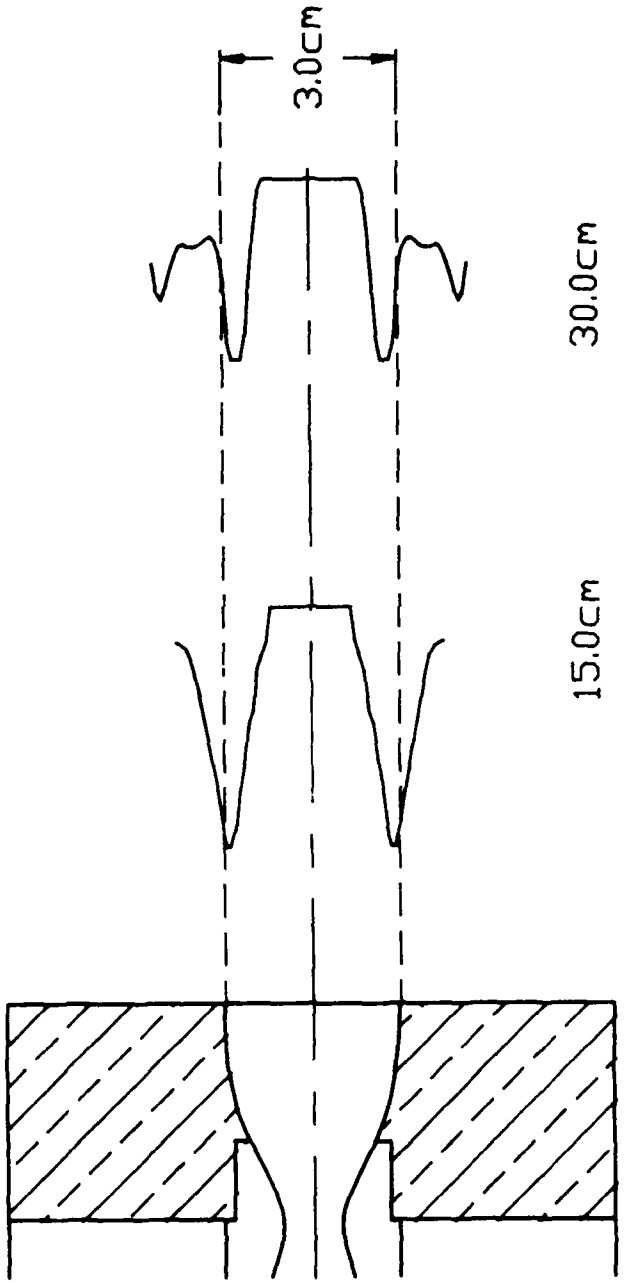

Figure 31. Electron density profiles inferred from Stark width measurements of argon and H_α indicates confinement of excitation in argon flow channel. Peak electron density observed was 2×10^{16} cm^{-3} and minimum detectable was 3×10^{15} cm^{-3}.

VIII. DISCUSSION

The basic result of the experimental program is that a plasma jet can successfully penetrate an atmosphere that provides radial confinement of the jet. The jets appear to propagate as coherent, albeit non-linear, structures that exhibit features in excellent qualitative agreement with numerical code predictions. In the experiments to date, the range of the jet approximately equals the product of penetration speed and pulse duration, with the jet penetrating tens of diameters into the target atmosphere during the pulse. The core flow diameter is maintained for the length of jet propagation.

Future experiments need to extend the penetration speed of the jet and the pulse duration in order to evaluate performance at higher energy densities and greater aspect ratios (range/diam). Such experiments will require higher current sources and longer current pulsetimes. The penetration speed of the jet should scale as the square root of the thrust per unit area of the arcjet source and, for electromagnetic thrusters, the speed will therefore scale linearly with the discharge current. Further development of the arcjet source is necessary to achieve satisfactory operation as the current level is increased, but can probably proceed adequately by experimental test and modification of simple devices. An interim possibility exists to attempt a very high current test by use of a crow-barred capacitor bank (vs LC-ladder network). Currents up to a few hundred kiloamperes would be possible for a few hundred microseconds by reconfiguring connections to the present 400 kJ capacitor bank. Useful data may be obtained by a such near term test in preparation for millisecond operation at current levels of several hundred kiloamperes utilizing the five-megajoule system components at the RDA Washington Research Laboratory.

There are a large number of parameters that must still be explored in order to develop scaling relations for jet propagation. Experiments are planned in which the arcjet mass flow rate

and target atmosphere pressure will be varied about the present successful operating point. In addition, the thrust density of the arcjet will be changed by varying the input current. The balance between scaling experiments to explore operating characteristics and higher power experiments to extend the performance of the jets into higher energy density regimes will depend on resource constraints and overall program requirements.

APPENDIX I

RELATIONSHIP OF JET FLOW SPEED TO PENETRATION SPEED FOR FINITE MACH NUMBERS

APPENDIX I

Relationship of Jet Flow Speed to Penetration Speed for Finite Mach Numbers

The flow near the jet nose of a propagating plasma jet is quite complex but may be divided into three regions: a shock that takes the atmosphere in front of the jet nose up to the penetration speed (at least on the exact centerline); a shock that reduces the jet flow speed to that of the nose structure; and a contact surface separating the shocked atmosphere flow from the shocked jet flow. To solve for details of the nose structure, the two-dimensional flow of the shocked atmosphere and jet must be matched. In principal, at very high Mach numbers, analytical solution may be possible since at least a portion of the flow may be very subsonic ($M \approx 0$) so incompressible flow techniques can be used. This is the approach used to obtain the shock stand-off distance from a blunt body in hypersonic flow. In the present case, however, the geometry of the contact surface ("blunt body") must be determined by the flow itself.

The relationship of the jet flow speed to the penetration speed may be formulated without regard to the detailed shape of the nose flow, if the condition of stagnated flow on the jet centerline is invoked (in the frame of the propagating jet). The stagnation pressures on either side of the contact surface must match on the centerline, so the Mach number of the incoming atmosphere flow can be related to the Mach number of the jet flow (in the frame for which the shocks are stationary).

The stagnation pressure of the atmosphere flow is:

$$p_{01} = p_a \left[1 + \frac{(\gamma_a - 1)}{2} M_J^2\right]^{\gamma_a/\gamma_a - 1}$$

where p_a is the atmospheric pressure (as set in the lab frame), $M_1 = u_p/c_a$ is the Mach number of the jet penetrating at

speed u_p (in the lab) into an atmosphere with sound speed c_a and specific heat ratio γ_a. Similarly, the stagnation pressure of the jet flow in the frame of the shocks is:

$$p_{04} = p_J \left[1 + \frac{(\gamma_J - 1)}{2} M_J^2\right]^{\gamma_J/\gamma_J - 1}$$

where the static pressure of the jet is p_J (which equals p_a by the radial force equilibrium of the jet), M_J is the jet Mach number (in the shock frame) and γ_J is the specific heat ratio of the jet material.

Across a shock, the flow stagnation pressure decreases, with the ratio of stagnation pressures given by (Liepmann and Roshko, Elements of Gasdynamics, p. 61):

$$\frac{p_{02}}{p_{01}} \left[1 + \frac{2\gamma}{\gamma+1} (M_1^2 - 1)\right]^{-1/(\gamma-1)} \left[\frac{(\gamma+1)M_1^2}{(\gamma-1)M_1^2 + 2}\right]^{\gamma/(\gamma-1)}$$

The relationship between jet Mach number and penetration Mach number is then obtained by matching stagnation pressures after the respective shock processes, and utilizing the radial force balance to equate p_J with p_a:

$$\left[1 + \frac{(\gamma_J - 1)}{} M_J^2\right]^{\gamma_J/\gamma_J - 1} \left[1 + \frac{2\gamma_J}{(\gamma_J+1)} (M_J^2 - 1)\right]^{-1/\gamma_J - 1} \left[\frac{(\gamma_J+1)M_J^2}{(\gamma_J-1)M_J^2+2}\right]^{\gamma_J/\gamma_J - 1}$$

$$= \left[1 + \frac{(\gamma_a - 1)}{} M_1^2\right]^{\gamma_a/\gamma_a - 1} \left[1 + \frac{2\gamma_a}{(\gamma_a+1)} (M_1^2 - 1)\right]^{-1/\gamma_a - 1} \left[\frac{(\gamma_a+1)M_1^2}{(\gamma_a-1)M_1^2+2}\right]^{\gamma_a/\gamma_a - 1}$$

Experimental measurements provide $M_1 = u_p/c_a$ and also the Mach number in the lab frame M_w of the jet flow, as observed by the oblique shock over a wedge in the flow. The relationship of the Mach number in the shock frame to that in the lab frame is:

$$M_J = \frac{u_J - u_p}{c_J}$$

$$= M_w - u_p/c_J \quad .$$

The measured values of M_W and u_p can then be combined with the calculated value of M_J to obtain the sound speed c_J in the jet flow. With this sound speed, the jet speed in the lab is $u_J = M_W c_J$, and estimates of the jet temperature can also be made ($T_J = m_J c_J^2/\gamma k$). In the shock frame, the jump conditions across the two normal shocks preserve the sum $(p + \rho u^2)$ in the shock frame for each fluid, so the relationship of u_p to u_J is still given by

$$\frac{u_p}{u_J} = \frac{\eta^{\frac{1}{2}}}{1+\eta^{\frac{1}{2}}}$$

for finite Mach numbers if the impulse functions are balanced on the same cross-sectional area. The present analysis merely provides a self-consistent way to obtain T_J and η from experimental data.

APPENDIX II

BOUNDARY LAYER GROWTH AROUND A PROPAGATING JET

APPENDIX II

BOUNDARY LAYER GROWTH AROUND A PROPAGATING JET

To estimate viscous drag effects on the propagation of a dense jet into the atmosphere, it is useful to consider the development of a boundary layer around a cylindrical body (representing the jet flow/contact surface) penetrating the atmosphere at uniform and constant speed. At the nose of the jet, a normal shock accelerates the atmosphere up to the speed of the contact surface in the manner of a hypersonic blunt body. The atmosphere at the jet nose thus compresses by a factor up to (γ_a+1/γ_a-1), where γ_a is the ratio of specific heats for the atmosphere. This compressed flow then spills over the edge of the blunt nose and expands to the equilibrium pressure of the surrounding atmospheric flow. The surrounding flow, which did not pass through the normal shock and expansion fan near the jet nose, is frictionally-coupled to the shock-accelerated flow.

In order to achieve a tractable model, the shock-accelerated flow will be considered as a cylindrical boundary with axial speed equal to the penetration speed ($u_b = u_p$). Compressibility and heat transfer effects are limited (arbitrarily) to the shock-accelerated flow, while the density of the surrounding atmosphere is assumed to be uniform and constant. The kinematic viscosity of this atmosphere is also taken to be constant. All of the complexity of the hypersonic merged layer (shock/viscous boundary with nonuniform temperature and chemistry) is ascribed to the shock-accelerated flow and provides a flow boundary condition for a much simpler surrounding flow that supplies the drag force of the atmosphere on the penetrating jet flow.

The time-dependent viscous diffusion of vorticity and axial momentum into the surrounding flow is treated as a cylindrical form of Rayleigh's problem (impulsive motion of a sheet) in order to calculate growth of the boundary layer ('momentum defect') thickness.

The basic equation for axial acceleration due to viscous coupling in cylindrical geometry is:

$$\frac{1}{\nu}\frac{\partial u}{\partial t} = \frac{1}{r}\left[\frac{\partial}{\partial r} r \frac{\partial u}{\partial r}\right]$$

where ν = kinematic viscosity (μ/ρ) assumed uniform and u = axial flow speed. In the same manner as Rayleigh's problem in rectangular geometry, similarity solution is again possible by substituting

$$\bar{u}(\bar{r},\bar{t}) = \bar{u}(Ar,Bt) = u(r,t)$$

in the partial differential equation,

$$\frac{1}{\nu} B \frac{\partial \bar{u}}{\partial \bar{t}} = \frac{A}{\bar{r}}\left[\frac{\partial}{\partial \bar{r}}\left[\frac{\bar{r}}{A}\frac{\partial \bar{u}}{\partial \bar{r}} A\right] A\right]$$

so

$$\frac{1}{\nu} B \frac{\partial \bar{u}}{\partial \bar{t}} = A^2 \frac{1}{\bar{r}}\frac{\partial}{\partial \bar{r}}\left[\bar{r}\frac{\partial \bar{u}}{\partial \bar{r}}\right]$$

which is the same as the original equation with a new kinematic viscosity $\nu^* = \nu A^2/B$. The stretching factor A can be eliminated in favor of a single arbitrary constant B:

$$u(r,t) = \bar{u}(\sqrt{B\nu^*/\nu}\, r,\ Bt)$$

With $\nu^* = \nu$, u is constant along parabolas in the rt-plane so:

$$u(r,t) = u\,(r/\sqrt{\nu t})$$
$$= u(y) \qquad , \text{ where } y = r/\sqrt{\nu t}$$

Substitution in the partial differential equation provides an ordinary differential equation:

$$y^2u'' + yu' + 1/2\ y^3u' = 0.$$

so

$$\frac{du'}{dy} = \frac{-(1 + y^2/2)}{y} u' \qquad ,$$

$$\ell n\, u' = \ell n\, y - y^2/4 \quad .$$

and

$$u' = \frac{k_1 e^{-y^2/4}}{y}$$

where k_1 is a constant to be determined. The axial speed as a function of y is then

$$u = k_1 \int \frac{e^{-y^2/4}}{y}\, dy + k_2$$

where k_2 is another constant of integration. The integral on the right can be transformed as:

$$\int \frac{e^{-y^2/4}}{y}\, dy = \frac{1}{2}\int \frac{e^{-y^2/4}}{(y^2/4)}\, d(y^2/4)$$

$$= \frac{1}{2}\int \frac{e^{-p}}{p}\, dp \quad .$$

At the boundary provided by the cylindrical penetrating jet flow, $r = r_b$, $u = u_b$ for any time t, so $k_2 = u_b$. Also, for any finite time t, the axial speed at $r \to \infty$ is zero, so

$$k_1 = \frac{-k_2}{\frac{1}{2}\int_{y_b^2/4}^{\infty} \frac{e^{-p}}{p}\, dp}$$

where $y_b = r_b/\sqrt{\nu t}$.

From Jahnke and Emde, Table of Functions (Dover, 1945) p.1,

$$-E_i(-x) = \int_x^{\infty} \frac{e^{-p}}{p}\, dp > 0 \quad ,$$

which is a type of logarithmic integral,

so,

$$k_1 = \frac{-u_b}{\frac{1}{2}\left[-E_i\left(\frac{-y_b^2}{4}\right)\right]}$$

With

$$\int_{y_b}^{Y} \frac{e^{-y^2/4}}{y}\, dy = \frac{1}{2}\left[\int_{y_b^2/4}^{\infty} \frac{e^{-p}}{p} dp - \int_{y^2/4}^{\infty} \frac{e^{-p}}{p} dp\right] ,$$

the axial speed at radius r and time t corresponding to $y = r/\sqrt{\nu t}$ is then:

$$u = u_b \left[1 - \frac{\left[-E_i(-y_b^2/4)\right] - \left[-E_i(-y^2/4)\right]}{\left[-E_i(-y_b^2/4)\right]}\right] ,$$

so

$$\frac{u}{u_b} = \frac{E_i(-y^2/4)}{E_i(-y_b^2/4)} .$$

The momentum in the boundary layer ('momentum defect') is:

$$P = \int_{r_b}^{\infty} \rho u \, 2\pi r dr$$

where ρ is the mass density of the surrounding atmosphere. From Jahnke and Emde (op. cit.) p. 4,

$$\int_0^x E_i(-mp)dp = xE_i(-mx) - \frac{1-e^{-mx}}{m} .$$

Thus, with m = 1,

$$\int urdr = 2u_b \nu t \int \frac{[-E_i(-y^2/4)]}{[-E_i(-y_b^2/4)]}\, d(y^2/4)$$

and

$$P = \frac{4\pi\rho u_b \nu t}{[-E_i(-y_b^2/4)]}\left[-1 - y_b^2/4\ [-E_i(-y_b^2/4)] + 1 + e^{-y_b^2/4}\right]$$

$$= 4\pi\rho u_b \nu t \left[\frac{e^{-y_b^2/4}}{-E_i(-y_b^2/4)} - \frac{y_b^2}{4}\right] .$$

The effective viscous-limited range R is defined as the value for $t = R/u_p$ for which the momentum defect equals the momentum of the atmosphere penetrated by the jet cross-section,

$P_b = \rho u_b \pi r_b^2$ (for an equal axial displacement of the jet nose and the boundary layer flow):

$$\frac{P}{P_b} = 1 = \frac{4}{y_b^2}\left[\frac{e^{-y_b^2/4}}{-E_i(-y_b^2/4)} - \frac{y_b^2}{4}\right] .$$

This condition is satisfied for $y_b = 1.562$, so

$$r_b = 1.562\left(\nu \frac{R}{u_p}\right)^{1/2}$$

defines a minimum jet radius needed to propagate a distance R before viscous effects dominate.

APPENDIX III

SCALING RELATIONSHIPS FOR DENSE PLASMA JET OPERATION

APPENDIX III

Scaling Relationships for Dense Plasma Jet Operation

To assess the regime of operation of a dense plasma jet for defense applications, it is useful to estimate the relationships of jet power, propagation range, jet diameter, and lethality of interaction with a target. Since the details of jet penetration through the atmosphere at hypersonic speeds and jet impingement on solid surfaces are quite complex, simple scaling relationships will require experimental tests to benchmark transport coefficients, ablation energies and speeds.

The jet power flux per unit area is given by:

$$\frac{P}{A_J} = (\rho_J u_J) \frac{u_J^2}{2} \quad ,$$

where the product of jet density ρ_J, exit speed u_J and exit area A_J is the mass flow rate from the jet source. In terms of the mass density ratio, $\eta = \rho_J/\rho_a$, and the jet penetration speed u_p, the jet power flux is:

$$\frac{P}{A_J} = \frac{1}{2} \rho_a u_p^3 \eta \left[1 + \frac{1}{\eta^{1/2}}\right]^3 \quad ,$$

where ρ_a is the mass density of the surrounding atmosphere. For specified values of ρ_a and u_p, the jet power flux is minimum when $\eta = 0.25$ (for which $\eta(1 + \eta^{-1/2})^3 = 6.75$).

The total jet power P is the product of power flux and area and can be calculated only if the necessary value of A_J is specified. To estimate A_J, it is useful to recognize that the basic momentum equation for the jet penetrating a radially-confining atmosphere provides a relationship between jet speed u_J and penetration u_p that is independent of cross-sectional area A_J. Diffusive phenomena such as viscous momentum transfer must be considered in order to obtain fundamental limits on the jet range and thereby to specify the initial jet area.

From Appendix II, the necessary jet radius r_J to achieve a range R before viscous effects dominate is given by:

$$r_J = 1.562\sqrt{\nu R/u_p}$$

$$= 1.562\left(\frac{\mu}{\rho_a}\frac{R}{u_p}\right)^{1/2} ,$$

where the quotient of viscosity μ and mass density ρ_a is the kinematic viscosity ν. The necessary minimum jet area is then:

$$A_J = \pi r_J^2$$

$$= 7.66\ \frac{\mu}{\rho_a}\frac{R}{u_p} .$$

The minimum total jet power for a penetration range R is therefore:

$$P = 3.83\ \mu R u_p^2\ \eta\ \left[1 + \frac{1}{\eta^{1/2}}\right]^3$$

$$= 25.87\ \mu R u_p^2 \quad , \quad \text{for } \eta = 0.25.$$

Note that this power is only weakly dependent on the density of the surrounding atmosphere since the coefficient of viscosity μ depends on density only indirectly (through the chemical state of the atmosphere). For air at sea level and 300° K, the standard atmosphere value for μ is about 2×10^{-5} kg/m^{-3}, so the jet power to achieve a range of 10 km at a penetration speed of 10 km/s would be about 517 MW. Table A provides values for other conditions along with the minimum jet diameters. (The use of a handbook value of μ continues the simplicity of the modeling in Appendix II and the assumption that the boundary layer growth of interest is well outside of the hypersonic merged layer around the jet core.)

If the jet can reach a target, it must be able to provide lethal damage in order to have useful defense application. Concern for lethality translates into a need for sufficient jet power flux to overheat a target surface, causing local ablation rapidly enough for severe impulsive loading. Such loading is

rapidly enough for severe impulsive loading. Such loading is usually expressed as the impulse per unit area which is the product of local pressure $\bar{p}$ and application of time δt (e.g., taps in cgs units), but should be further specified to local pressure loadings above one kilobar and pulse times below 100 μs. An impulse per unit area above 1000 nt-s/m^2 (10 ktaps) is probably a useful goal.

The local pressure due to the jet impinging on a target surface is largely a result of target ablation, rather than the dynamic pressure of the jet:

$$\bar{p} = \left(\frac{P}{A_J}\right) \frac{u_A}{Q} \quad ,$$

where u_A is the ablation speed of the target material and Q is the energy absorbed per unit mass of ablatant. For a penetration speed u_p = 10 km/s, sea-level mass density, ρ_a = 1.22, and η = 0.25, the jet power per unit area is 4.1 x 10^{12} w/m^2. If u_A = 10 km/s and Q = 10 MJ/kg, then $\bar{p}$ = 41 kbar.

A range of R = 10 km at u_p = 10 km/s requires a minimum jet diameter of $2r_J$ = 1.4 cm. An element of target surface crossing the jet at a speed of 2 km/s (~ Mach six) would experience the pressure loading for about δt = 7 μs. The total impulse per unit area given to the surface element would then be $\bar{p}\delta t$ = 2.87 x 10^4 nt-s/m^2 (= 287 ktaps). The details of jet interaction with the target surface are quite complex so it is not straightforward to declare that the computed impulse for unit area will actually be obtained. It is useful to note, however, that the speed of the jet flow onto the target (vs the jet penetration speed to reach the target) is about a factor of three higher than escape velocity (~ 10 km/s), while the jet flow density may be several times higher than usual for re-entry braking. The target surface would thus be exposed to local flow loadings (1/2 ρu^3) that may be two orders of magnitude higher than atmospheric re-entry design values. In terms of the desired range, penetration speed and total jet power, the impulse per unit area relationship is:

$$\theta = \frac{2}{\pi} \frac{Pu_A}{Q} \frac{1}{r_j}$$

$$= 0.4 \frac{Pu_A}{Q} \left[\frac{\rho_a u_p}{\mu R}\right]^{1/2}$$

or

$$\theta = 10.35 \ (u_A/Q)(\mu \rho_a R)^{1/2} \ u_p^{5/2} \ , \quad \text{for } \eta = 0.25.$$

Thus, lethality expressed as impulse per unit area improves with operating density (i.e., lower altitude) and longer range (associated with higher total power). Table A provides additional sample values for pressure loading, pulse duration and impulse per unit area.

Table A. Sample Values for Dense Plasma Jet Operation

	Design A R = 10 km u_p = 5 km/s	Design B R = 20 km u_p = 10 km/s	Design C R = 40 km u_p = 10 km/s
Jet Power $\mu = 2 \times 10^{-5}$ kg/m-s	129 MW	1.0 GW	2.0 Gw
Jet Diameter H = 0 km (H = 20 km)	1.8 (6.6) cm	1.8 (6.6) cm	2.5 (9.3) cm
Target Interaction Time u_t = 2 km/s	9 (33) μs	9 (33) μs	12.5 (46.5) μs
Target Over-Pressure $u_a/Q = 10^{-3}$	5.1 (0.38) kbar	39 (2.9) kbar	41 (3.0) kbar
Impulse per Unit Area	46 (12.5) ktaps	351 (96) ktaps	513 (140) ktaps
MPD Arcjet Current	293 kA	577 kA	816 kA
MPD Voltage	440 V	1.7 kV	2.5 kV